doi:10.20944/preprints202102.0537.v1

A review of damage, void evolution and fatigue life prediction models

Hsiao Wei Lee, and Cemal Basaran*

Dept. of Civil, Structural and Environmental Engineering, University at Buffalo

*Corresponding author cjb@buffalo.edu

Keywords: void evolution, degradation, damage, fatigue, fatigue-life, failure prediction, entropy, thermodynamics, unified mechanics

ABSTRACT

This paper aims to provide an overall review of degradation, damage evolution and fatigue models in the literature of various engineering materials, mostly metals, and composites.

1. Introduction

The degradation, damage evolution and fatigue behavior of materials are closely related to structural serviceability and safety. It is well-understood that engineering materials such as metals and composites have different micro-mechanisms, degradation process, damage accumulation and different failure modes that are dependent on many factors. For example, when the strain rate is in the range from 10^{-6} to 10^{-5} s^{-1}, creep can be a dominant mechanism; when the rate of strain is in the neighborhood of 10^{-4} to 10^{-3} s^{-1}, the response is quasi-static, which allows the measurements of (quasi-static) stress-strain curves using universal test machines under constant strain rates. The strain-rate regime of 10^{3} s^{-1} and beyond is generally regarded as the high strain rate range, where inertia terms, wave propagation influences and thermal effects (e.g. adiabatic shear banding) become important and need to be considered[84].

In the literature damage evolution and fatigue life prediction models can be classified in two categories: Empirical models which established under the framework of Newtonian mechanics (this also includes Hamiltonian and Lagrangian mechanics). Regardless of different ways used to characterize the damage evolution with equations and a number of parameters, it primarily relies on test data curve for fitting for the empirical void/damage evolution function. Examples include GTN model[85], Rice-Tracey model[86], Gunawardena model[87], the well-known strain rate dependent Johnson-Cook (JC) damage model[88], some other micro-mechanism based damage models and models based on continuum damage mechanics (CDM) theory. These empirical models are popular for engineering applications due to their simplicity, but the identification of parameters is costly, time consuming and lacks any scientific basis because they lack physical and mathematical foundations[89].

The physics-based models, on the other hand, as the name suggests are based on the physical foundations and do not require curve fitting empirical functions. They can be classified under the framework of Unified Mechanics Theory, which modifies the universal laws of motion of Newton by incorporating second law of thermodynamics directly into Newton's laws at the ab-initio level[90]. As a result, governing differential equations of any system automatically include energy loss, entropy generation and degradation of the system in a non-empirical way. The UMT based models are pure physics based and do not require any curve fitting to a test data for evolution of void/damage. Thermodynamic fundamental equation and the second law of thermodynamics controls the evolution of damage along the fifth axis [Thermodynamic State Index axis].

In the following sections, some recent models for various engineering materials are reviewed. They are categorized based on their approach as well as the type of material being investigated. In section 2, empirical models including Gurson–Tvergaard–Needleman (GTN) type models, Johnson-Cook (JC) type models, microplasticity models, and some other empirical models are introduced and discussed. In section 3, physics-based models using unified mechanics theory are presented. Experimental verifications of physics-based models without simulations are also included in this section.

2. Empirical models

2.1 Gurson–Tvergaard–Needleman (GTN) type models

The micro mechanical model developed by Gurson–Tvergaard–Needleman[85][101] is widely used for the prediction of ductile fracture on the basis of nucleation, growth and coalescence of voids in materials. However, it is only applicable to relatively high stress conditions. For shear loading, the GTN model significantly overestimates the carrying capacity of materials[7][11][96]. Although it does not apparently consider the effect of strain rate, the model calculates the strain rate and consider its effect on the void growth depending on the loading rate and the predefined solution time[89]. Moreover, the model is suitable for the relatively low strain rates, while at higher strain rates, such as impact problems, the numerical simulation results are not accurate. Many researchers have adopted the GTN model and performed further modification to account for the fracture mechanism due to shear, in order to predict ductile fracture under a low level of stress triaxiality. Some researchers combined the GTN model with

Johnson-Cook model considering the strain rate to better describe the ductile fracture process under high strain rate of loading. In the following sub-section those modified models are introduced.

Acharya and Dhar [2008] predicted the ductile failure of pipe using GTN model. An attempt has been made to fine tune the values of some of the GTN model's empirical curve fitting parameters by comparing the simulated results with the experimental results at the specimen level (axisymmetric tensile bar and compact tension specimens). An elastic–plastic finite element code has been developed together with GTN model for void nucleation and growth. The GTN model can be expressed in the following form. The yield function equation is given by

$$\phi = (\frac{\sigma_{eq}}{\sigma_m})^2 + 2q_1 f^* \cosh\left(-\frac{3}{2}\frac{q_2\sigma_h}{\sigma_m}\right) - (1 + q_3 f^{*2}) = 0 \tag{1}$$

where q_1, q_2, q_3 are empirical curve fitting parameters, σ_{eq} is the von Mises equivalent stress, σ_h is the hydrostatic stress, σ_m is the flow stress that characterizes the microscopic stress state of the matrix. f^* is the total effective void volume fraction proposed by Tvergaard and Needleman to account for the onset of void coalescence[101]:

$$f^*(f) = \begin{cases} f & f \le f_c \\ f_c + \dfrac{\left(\frac{1}{q_1}\right) - f_c}{f_f - f_c}(f - f_c) & f > f_c \end{cases} \tag{2}$$

where the void volume fraction f represents the damage parameter, f_c is the critical value of porosity at the onset of void coalescence. f_f is the failure value of void volume fraction. When the void volume fraction f reaches to f_f , the material loses its load carrying capacity. f_c and f_f are obtained by empirical curve fitting to a test data.

The cumulative equivalent plastic strain increment is defined by

$$\dot{\varepsilon}^p_{eq} = \frac{\sigma : \dot{\varepsilon}^p}{(1 - f)\sigma_m} \tag{3}$$

The damage evolution is divided into two parts: the growth of existing voids and the nucleation of new voids, which is expressed as follows

$$\dot{f} = \dot{f}_{growth} + \dot{f}_{nucleation}, \quad \dot{f}_g = (1 - f)\dot{\varepsilon}^p_{kk} \ , \ \dot{f}_n = A\dot{\varepsilon}^p_{eq} \tag{4}$$

where A is a function of ε^p_{eq} in some statistical sense.

Xue [2007] studied the constitutive modeling of void shearing effect in ductile fracture of porous materials. A new damage variable was introduced; first to replace

the widely used void volume fraction and second to incorporate the additional damage due to void shearing. In the modification, the void shearing damage effect, which was missing previously in the GTN model, was incorporated in the damage evolution.
The evolution of the damage described in a rate form is given by

$$\begin{gathered} D = K_D(q_1\dot{f} + \dot{D}_{shear}) \\ \dot{D}_{shear} = q_3 f^{q_4} g_\theta \varepsilon_{eq} \dot{\varepsilon}_{eq} \end{gathered} \tag{5}$$

where q_1, q_3, q_4 are empirical constants, K_D is the empirical damage rate coefficient, f is the void volume fraction, D_{shear} is damage associated with void shearing, g_θ is assumed to represent the azimuthal dependence on an octahedral plane, ε_{eq} is the equivalent strain. Same approach was used by Youbin Chen et al [2016] , where they studied the damage induced by spherical indentation deformation by using a modified GTN model.

Jin et al[2008] investigated the mechanical properties and damage mechanism of 5A06 aluminum alloy welded joint under thermal cycling condition. Microstructural and fractographic observations demonstrate that void nucleation around the second phase particles is the dominant factor for performance decrease. The theoretical results of micromechanical analysis have been introduced into the empirical Gurson void nucleation equations to characterize the evolution of void-damage under thermal cycling condition. The modified void nucleation model developed here provides a quantitative description of thermal stress assisted voiding under thermal cycling conditions. However, it must be noted that only the strain-controlled nucleation mechanism is considered in the study.
The accumulated plastic strain rate of the matrix due to thermal cycling is given as

$$\dot{\varepsilon}^p_{eq} = \frac{\varepsilon^{pl,(N_T+1)} - \varepsilon^{pl,N_T}}{N_T} = \begin{cases} \dfrac{2\sigma_y(1-v_1)}{E_1}\left[\left(\dfrac{r_p}{r}\right)^3 - 1\right] & N_T = 1 \\ \dfrac{4\sigma_y(1-v_1)}{E_1 N_T}\left[\left(\dfrac{r_c}{r}\right)^3 - 1\right] & N_T \geq 2 \end{cases} \tag{6}$$

where E_1 is Young's modulus of the alloy matrix, r is the radius of the spherical unit cell model containing a second phase particle, r_p is the radius of the plastic region. A zone of reversed plastic flow will form under the temperature reversal. r_c is the radius of the reversed plastic region, N_T is the cyclic period, σ_y is the yield stress in the interface and the neighboring matrix material.
The modified strain-controlled void nucleation equation is therefore given as

$$\dot{f}_n = A\dot{\varepsilon}^p_{eq} \tag{7}$$

Using GTN model, Linse et al[2012] simulated the fracture of a typical steel pressure vessel using a gradient-enriched ductile damage model based on dilatational strain. In the model the evolution of damage is controlled by introducing an internal length scale that represents a characteristic material parameter independent of the mesh size. The investigations are focused on the evolution of ductile damage and stress state at the crack tip. The results show that the model captures the different stages of crack initiation and propagation realistically. Their work includes a non-local modification: Motivated by the approach of generalized continua, the GTN continuum damage model is modified by replacing the dilatational part of the plastic strain rate $\dot{\varepsilon}_p$ by its non-local spatial average $\dot{\bar{\varepsilon}}_p$ in the empirical damage evolution equation for the growth of existing voids

$$\begin{gathered} \dot{f}_G^{nl} = (1-f)\dot{\bar{\varepsilon}}_p \\ \dot{f} = \dot{f}_G^{nl} + \dot{f}_N \\ \bar{\varepsilon}_p - c\nabla^2\bar{\varepsilon}_p : \boldsymbol{I} = \varepsilon_p \end{gathered} \tag{8}$$

where $\dot{f}_g^{nl}$ is the non-local modification of void growth rate, $\dot{f}$ is the empirical rate of damage evolution, $\dot{f}_N$ is the nucleation of new voids, ε_p is the volumetric plastic strain, $\bar{\varepsilon}_p$ is the non-local volumetric plastic strain, c is a non-local length parameter.

The GTN model has its limitations as it ignores the fracture mechanism due to shear. A number of papers have been published to develop modified GTN models by adding a function to capture the fracture at low stress triaxiality, Xue's shear mechanism [7] and Nahshon-Hutchinson's shear mechanism [11] have received most attention. Xu et al[2013] used the modified Gurson model for the failure behavior of the clinched joint on Al6061 sheet. In this work, Nahshon-Hutchinson's shear mechanism[11] is used because this model shows a good correlation between the simulation and experimental test data. In addition, it has shown improved accuracy of fracture over Xue's shear mechanism [7] under tensile/shear loading conditions. This extended empirical damage evolution function considers a nondimensional metric of stress state ω(σ) with an empirical shear damage coefficient k_ω and uses a modified GTN damage, as follows

$$\dot{f}_g = (1-f)\dot{\varepsilon}_{kk}^p + k_\omega \frac{f\omega(\sigma_{ij})}{\sigma_e} S_{ij}\dot{\varepsilon}_{ij}^p \tag{9}$$

where S_{ij} is the stress deviator, $\omega(\sigma_{ij})$ is the non-dimensional metric of stress state, σ_e is the von Mises equivalent stress.

Using the same approach, Gatea et al[2017] simulated ductile fracture in Single Point Incremental Forming(SPIF) process due to void nucleation and coalescence with results compared with the original GTN model. A combined approach of experimental testing and SPIF processing was used to validate finite element results of the shear modified Gurson–Tvergaard-Needleman damage model.

Malcher et al[2014] proposed a new formulation to improve the original GTN model, regarding its ability to predict ductile fracture under a low level of stress triaxiality.

Firstly, a new shear mechanism was proposed that is a function of the equivalent plastic strain, stress triaxiality and Lode angle. This mechanism can capture the elongation and rotation of microdefects, when shear loading condition is present. Furthermore, a new micro-defect nucleation mechanism was proposed which is responsible for triggering the evolution of the shear damage parameter, since the new mechanism is independent on the volume void fraction. Then, the new empirical damage parameter was coupled with GTN empirical constitutive formulation in such a way that only affects the deviatoric stress contribution. Thus, the new model has two new independent empirical damage parameters: first one affecting the hydrostatic stress component and the other affecting the deviatoric stress component.

$$\dot{D} = g_0 \frac{D_N}{S'_N\sqrt{2\pi}} \exp\left[\frac{-1}{2}\left(\frac{\bar{\varepsilon}^p - \varepsilon'_N}{S'_N}\right)^2\right]\dot{\bar{\varepsilon}}^p + |g_0|^{\frac{1}{|\eta|+k}} q_6 \dot{D}_{shear}$$

$$\dot{D}_N = g_0 \frac{D_N}{S'_N\sqrt{2\pi}} \exp\left[\frac{-1}{2}\left(\frac{\bar{\varepsilon}^p - \varepsilon'_N}{S'_N}\right)^2\right]\dot{\bar{\varepsilon}}^p \tag{10}$$

$$\dot{D}_{shear} = \begin{cases} q_3 D^{q_4} \bar{\varepsilon}^p \dot{\bar{\varepsilon}}^p & Xue's\ mechanism \\ \dfrac{1}{\ln\sqrt{1/\chi}}\left(\dfrac{3\bar{\varepsilon}^p}{1+3\bar{\varepsilon}^{p2}}\right)\dot{\bar{\varepsilon}}^p & Butcher's\ mechanism \end{cases}$$

where q_3, q_4, q_6 are empirical constants, g_0 is a Lode angle dependence function, $\dot{D}$ represents the evolution of the shear damage, $\dot{D}_N$ represents its nucleation and $\dot{D}_{shear}$ is the evolution of shear effects, ε'_N and S'_N are the mean strain for void nucleation and its standard deviation. The variable $\bar{\varepsilon}^p$ represents the equivalent plastic strain and $\dot{\bar{\varepsilon}}^p$ is the rate of the accumulated plastic strain. η is the stress triaxiality parameter, k is a numerical constant that needs to be calibrated for each material by curve fitting, χ is the ligament size ratio defined for two- or three-dimensional problems.

Wang et al[2017] analyzed the tearing failure of ultra-thin sheet-metal including size effect in blanking process based on modified GTN model. The experiments suggested that void growth was suppressed around the narrow region due to the relatively low-stress triaxiality. The typical failure phenomena were exhibited in the form of tearing, which may imply that the conventional GTN model fails to predict such shearing domination failure. Therefore, a modified GTN model based on Lode parameter was tested to describe the failure mechanism.

Shear modified GTN model

$$\phi = \left(\frac{\sigma_{eq}}{\sigma_m}\right)^2 + 2q_1 f^* \cosh\left(-\frac{3}{2}\frac{q_2\sigma_h}{\sigma_m}\right) - (1 + (q_1 f^* + D_s)^2 - 2D_s) = 0 \tag{11}$$

$$D = q_1 f^* + D_s, \quad D_s = (\frac{\varepsilon_q^m}{\varepsilon_f^s})^n, \quad \dot{D}_s = \psi(\theta, T^*) \frac{n D_s^{\frac{n-1}{n}}}{\varepsilon_f^s} \dot{\varepsilon}_q^m$$

in which σ_{eq} is the von Mises equivalent stress, σ_h is the hydrostatic stress, and σ_m is the flow stress that characterizes the microscopic stress state of the matrix, f^* is the total effective void volume fraction, D_s is an empirical shear damage parameter, ε_q^m is the equivalent plastic strain of material matrix, ε_f^s is the failure strain under pure shear state, n is an empirical weakening exponential larger than one, $\psi(\theta, T^*)$ is an empirical weight factor.

Chen et al[2018] proposed a dislocation density based viscoplastic constitutive model coupled with damage to investigate a single impact loading process for TWIP (twinning induced plasticity) in steels. To predict the damage evolution in these ductile steels, the Gurson–Tvergaard–Needleman (GTN) yield criterion is combined with the dislocation density-based model. The obtained results allows for predicting the induced residual stress, plastic strain and damage fields. The results show that the maximum compressive residual stress reaches up to about 650 MPa when the impact velocity is 4 m/s. The damage area generated by single impact loading is annular and the indent center is not affected by damage.

During hot working, internal damage of the workpiece is not only controlled by the stress state, but also by time- and temperature-dependent softening processes such as recovery and recrystallization. These processes may be used to delay or prevent damage initiation and hence to improve part performance. Bambach and Imran[2019] proposed a new damage initiation model taking the interaction of dynamic recrystallization and decohesion into account. The criterion is integrated into the GTN model for porous plasticity. Based on the model and experimental studies, damage control by optimized strain rate profiles is investigated and material-dependent factors for damage control are discussed. Their empirical evolution function is given by

$$\dot{f}_n = \sigma_Y \frac{\dot{\varepsilon}\sqrt{d}}{K_{IC}} f\{0.177 - a_1\xi - a_2\xi^2 + b_1|\eta|\} \tag{12}$$

$\dot{f}_n$ is the growth of void nucleation, K_{IC} is the fracture toughness, $\dot{\varepsilon}$ is the plastic strain rate, ξ is a normalized third stress invariant, d, a_1, a_2 and b_1 are curve fitting parameters.

The fracture analysis of shape memory alloys in martensite and austenite phase based on the voids behavior by incorporating GTN model has also been studied recently[162], [163]. Bahrami et al[2019] proposed a constitutive model to investigate the pseudoelastic-plastic behavior of the shape memory alloys, SMAs, up to fracture. The proposed model is based on the Boyd and Lagoudas phase transformation model[167] which is extended to take into account the plastic deformation and the fracture behavior of the SMAs by using the Gurson-Tvergaard-Needleman (GTN) model shown in Eq (1-4).

2.2 Johnson-Cook (JC) type models

An empirical constitutive relation developed by Johnson and Cook (J–C)[88] is widely used to capture strain rate sensitivity of metals. The model proposed by Johnson and Cook is used to simulate the damage evolution and predict failure in many engineering materials. Wang et al[2019] proposed a material model based on the Johnson-Cook model considering the strain rate combined with void nucleation and coalescence in the GTN model to better describe the ductile fracture process of steel and predict the structural deformation damage during ship collisions and grounding accidents. The ASIS(association for structural improvement of shipping industry) test numerical simulation results of the Johnson-Cook GTN model are also compared with the lab test results, and the accuracy of the model subjected to shear loading is validated. Therefore, the model can predict structural deformation damage in ship collision and grounding simulations.

Li et al[2014] developed a 3D FEM model to simulate the formation and predict the sizes of cracks generated by inappropriate laser shock peening (LSP) processing in airfoil specimens in order to avoid producing subsurface cracks. This model was fully considered with the plastic and fracture behaviors at high strain rate by using both JC plastic and fracture models.

Johnson-Cook plastic model is given by

$$\sigma = (A + B(\varepsilon^{pl})^n)\left[1 + C \times \ln\left(\frac{\dot{\varepsilon}}{\dot{\varepsilon}_0}\right)\right]\left[1 + D \times (\frac{T - T_0}{T_0})^m\right] \tag{13}$$

Johnson-Cook empirical damage initiation criterion is given by

$$\bar{\varepsilon}_f^{pl} = [d_1 + d_2 \exp(-d_3\sigma^*)][1 + d_4 \ln(\frac{\dot{\bar{\varepsilon}}^{pl}}{\dot{\varepsilon}_0})] \times (1 + d_5 T^*) \tag{14}$$

where σ is the stress; ε^{pl} is the plastic strain; A is the initial yield stress; $\dot{\varepsilon}_0$ is the reference strain rate, T_0 is the reference temperature; σ^* is the dimensionless pressure-stress ratio, $\dot{\bar{\varepsilon}}^{pl}$ is plastic strain rate. T^* is the homologous temperature, B, n, C, D, and m are empirical coefficients, d_1, d_2, d_3, d_4, and d_5 represent different empirical failure parameters obtained by curve fitting to test data. The simulated crack sizes and locations in the airfoil coupon models are consistent with the experimental results.

Jeunechamps and Ponthot[2013] established an efficient 3D implicit approach for the thermomechanical simulation of elastic–viscoplastic materials subjected to high strain rate. The elasto-viscoplastic model is established by the coupling between the JC model and the Perzyna viscosity model.

Nam et al[2014] investigated the crack tip stress and strain fields at crack initiation of A106 Gr. B carbon steels under high strain rates. Three different strain rate tensile tests (4 x 10^{-4} s^{-1}, 3.4 s^{-1} and 11.6 s^{-1}) are fitted using Johnson-Cook model. Results show that applied strain rate and strain rate at characteristic length have similar values as in the CT(compact tension) specimen simulation result. Nam et al[2015] also proposed to implement ductile fracture simulation based on the energy. The energy based ductile fracture model determines the incremental damage in terms of stress triaxiality and fracture strain energy for dimple fracture using tensile test with FEM technique.

$$W_f = \left[Aexp\left(-C\frac{\sigma_m}{\sigma_e}\right) + B\right][1 + D\ln\left(\frac{\dot{\varepsilon}}{\dot{\varepsilon_0}}\right)] \quad (15)$$

Where W_f is the fracture strain energy for dimple fracture, σ_m/σ_e is the stress triaxiality, $\dot{\varepsilon}$ is the equivalent plastic strain rate, $\dot{\varepsilon_0}$ is the reference strain rate and A, B, C, D are empirical curve fitting constants.

Chen et al [2018] studied the mechanical behavior of the corroded high strength reinforcing steel bars under static and dynamic loading. High strength reinforcing steel bars were corroded by using accelerated corrosion methods and the tensile tests were carried out under different strain rates. Based on the test results, reduction factors were proposed to relate the tensile behaviors with the corrosion degree and strain rate for corroded bars. A modified Johnson-Cook strength model of corroded high strength steel bars under dynamic loading was proposed by considering the influence of corrosion degree.

$$\begin{cases} \alpha_A = \dfrac{A}{A_0} = 1 - k_A\eta_s \\ \alpha_B = \dfrac{B}{B_0} = 1 - k_B\eta_s \\ \alpha_C = \dfrac{C}{C_0} = 1 - k_C\eta_s \end{cases} \qquad \sigma = (A + B(\varepsilon^{pl})^n)\left[1 + C \times \ln\left(\frac{\dot{\varepsilon}}{\dot{\varepsilon_0}}\right)\right] \quad (16)$$

where η_s is the corrosion degree, A, B, and C are curve fitting parameters of corroded steel bars and A_0, B_0, and C_0 are curve fitting parameters of the J-C model of the uncorroded steel bars. k_A, k_B, k_C are curve fitting parameters also determined from test data.

Chen et al[2018] investigated the ductile damage behaviors of Ti-6Al-4V alloy for high strain rate compression tests over a wide range of strain rates and temperatures by a combined experimental and numerical approach. A coupling JCM(modified Johnson-Cook) plastic and energy density-based damage model were developed to characterize the whole range of flow stresses, including the plastic, failure initial strain and damage evolution

$$\sigma = (A + B\phi(\varepsilon^{pl})^n)\left[1 + C \times \ln\left(\frac{\dot{\varepsilon}}{\dot{\varepsilon_0}}\right)\right]\left[1 - (\frac{T - T_f}{T_m - T_f})^m\right]$$
$$\phi(T) = (\frac{T_0 - T/2}{T_0})^{n_2} \tag{17}$$

where A, B, C, n, m and n_2 are curve fitting empirical parameters. $\phi(T)$, a temperature dependent empirical function which is related to microstructure evolution, was introduced into the original JC model to characterize the temperature dependent work hardening behavior in flow curves. σ is the equivalent plastic flow stress, $\dot{\varepsilon}$ is the equivalent plastic strain rate, $\dot{\varepsilon_0}$ is the reference strain rate, T_f and T_m are, respectively, workpiece ambient and melting temperature. T_0 is a critical temperature related with microstructure evolution.

Wang et al[2019] investigated the deformation behaviors of superalloy GH3536 over a wide range of temperatures (298 K–1073 K) and at strain rates (0.1 s^{-1}–5200 s^{-1}). The investigation about the fracture behavior was also performed over a temperature range of 298 K–1073 K, strain rate range of 0.001 s^{-1}–5000 s^{-1} and stress triaxiality range of 0.6–1.1. According to the temperature and strain rate dependences of the deformation behavior, the original Johnson-Cook constitutive model was unable to describe such behavior. A modified J–C constitutive model was developed to accurately describe the deformation behavior of GH3536 superalloy, and modified J–C fracture criterion was proposed to accurately characterize the fracture behaviors of GH3536.

$$\sigma = \left\{A + B_1(1 - B_2 \ln(\dot{\varepsilon}^*))\left[1 + B_3 \times \ln\left(\frac{T}{T_r}\right)\varepsilon^n\right]\right\}$$
$$\left[1 + C_6 \ln(\dot{\varepsilon}^*) + C_7\left(\frac{1}{C_8 - \ln(\dot{\varepsilon}^*)} - \frac{1}{C_8}\right)\right](1 - DT^{*m}) \tag{18}$$

where A, B_1, B_2, B_3, n, m, D, C_6, C_7 and C_8 are curve fitting material parameters, $\dot{\varepsilon}^* = \dot{\varepsilon}/\dot{\varepsilon_0}$ is the dimensionless strain rate, $T^* = (T - T_f)/(T_m - T_f)$is homologous temperature.

With the advent of advanced testing techniques such as laser-induced particle impact test, it is possible to study materials mechanics under extremely high deformation rates. Wang and Hassani [2020] induced ultra-high strain rates in the range of 10^6 – 10^{10} s^{-1} in spherical microparticles of commercially pure titanium impacting a rigid substrate. They recorded impact-induced deformation of the microparticles in real-time and simulated the deformation using a finite element approach and two constitutive equations of Johnson–Cook and Zerilli–Armstrong. By comparing the deformed geometries from experimental data and simulated results, they evaluated the capability of the two constitutive equations—originally calibrated at 10^3 – 10^4 s^{-1} to describe deformation at ultra-high strain rates. Being mechanistically based, the Zerilli–Armstrong model was found to have a better performance than the Johnson–Cook model al higher strain rates. Zerilli–Armstrong model is given by

$$\sigma_y(T,\varepsilon,\dot{\varepsilon}) = C_0 + B_0\varepsilon^{C_n}\exp[-\alpha_0 T + \alpha_1 T ln(\dot{\varepsilon})] + B\exp[-\beta_0 T + \beta_1 T ln(\dot{\varepsilon})] \quad (19)$$

(For HCP metals)

where ε is the equivalent plastic strain, $\dot{\varepsilon}$ the plastic strain rate, T is the temperature, C_0, B_0, C_n, α_0, α_1, B, β_0, β_1 are curve fitting parameters. Here, C_0 is the athermal component of the yield strength of the material. B_0 and C_n are strain hardening constants. α_0 and β_0 are thermal softening parameters. Finally, α_1 and β_1 are strain rate sensitivity parameters.

Zhang et al[2020] reported the necking evolution of a near a Ti3Al2.5 V at high strain rates. The experimental results at different strain rates are used to determine a suitable constitutive model for finite element simulations of the dynamic tensile tests. The combined JC-KHL(Johnson Cook-Khane Huange Liang) model (or CJK) is proposed to describe the constitutive response of Ti3Al2.5 V. The CJK model predicts the macroscopic force-time history, true strain rate evolution and true stress-strain data with good agreement compared to the experimental measurements.

$$\sigma = [A + B\left(1 - \frac{\ln(\dot{\varepsilon}/\dot{\varepsilon}_0)}{\ln D_0^P}\right)^{n_1}(\varepsilon_p)^{n_0}](1 + C\ln(\frac{\dot{\varepsilon}}{\dot{\varepsilon}_0}))(\frac{T_m - T}{T_m - T_f})^m \quad (20)$$

where σ is the true stress, ε_p is the plastic strain, $\dot{\varepsilon}_0$ is a reference strain rate and D_0^P is an upper bound strain rate chosen arbitrarily. The curve fitting constants are A, B, C, m, n_1 and n_0. T, T_f and T_m are current, reference and melting temperatures.

Chiyatan and Uthaisangsuk[2020] investigated the effects of strain rate on mechanical properties and fracture mechanism of ferritic-martensitic dual phase (DP) steel grades 780 and 1000 by both experiments and micromechanics-based modeling. FE simulations using 2D representative volume elements (RVEs) were conducted for investigating microstructure effects on local deformation and damage of DP steels under varying strain rates. Macroscopic flow curve model is a combination of Swift-Voce hardening law and Johnson-Cook (JC) rate-dependent model

$$\sigma[\varepsilon,\dot{\varepsilon}] = (D\{A(\varepsilon_0 + \varepsilon^n)\} + (1-\alpha)\{B + Q(1 - \exp[-\beta\cdot\varepsilon])\})(1 + C\ln(\frac{\dot{\varepsilon}}{\dot{\varepsilon}_0})) \quad (21)$$

For the first term of Eq. (21), A, ε_0, n, B, Q, β are the Swift and Voce curve fitting material parameters, and the parameter $0 \le D \le 1$ is a weighting coefficient. The second term is JC strain rate hardening equation including the parameters C and the reference strain rate $\dot{\varepsilon}_0$. Flow curve of observed phase constituents at different strain rates were described by using a dislocation-based theory and local chemical composition in combination with the Johnson-Cook (JC) hardening model

$$\sigma[\varepsilon,\dot{\varepsilon}] = (\sigma_0 + \Delta\sigma + \alpha M\mu\sqrt{b}\sqrt{\frac{1-\exp(-Mk_r\varepsilon)}{k_r L}})(1 + C\ln(\frac{\dot{\varepsilon}}{\dot{\varepsilon}_0})) \quad (22)$$

where σ and ε are the von Mises stress and equivalent plastic strain, respectively. The first term σ_0 represents the Peierls stress and the effect of alloying elements in the solid solution state. The second term, $\Delta\sigma$ described the material strengthening by precipitation or carbon in solution. The last term demonstrated the effect of dislocation strengthening and material softening, which contained the material constant α, Taylor factor M, shear modulus μ, Burger's vector b for both phases. Moreover, the recovery rates k_r and dislocation mean free path L of each phase were defined separately. The local crack mechanisms in DP microstructures were described by individual empirical damage criteria for each phase based on the rate-dependent empirical JC failure model.

2.3 Microplasticity models

Besides the studies in macroscopic or continuum scale, there are many studies that focus on atomic-scale modeling of the void nucleation, growth, and coalescence, or those focus on crystal plasticity in meso-scale to unveil the fatigue hotspots, fatigue crack nucleation and fatigue life prediction.

Wan et al[2016] investigated microstructural stress distributions and fatigue hotspots in polycrystalline copper using HR-EBSD (High Resolution- Electron Backscatter Diffraction) and computational crystal plasticity. HR-EBSD studies on a deformed copper polycrystal have been carried out to quantify the microstructural residual stress distributions, and those of stress state of importance in defect nucleation. Crystal plasticity analysis of a representative, similarly textured, model polycrystal has been carried out showing that the experimental distributions of microstructural residual stress components, effective stress, hydrostatic stress and stress triaxiality are well captured. A stored energy criterion for fatigue crack nucleation indicates that preferential sites for fatigue crack nucleation are local to grain boundaries (as opposed to triple junctions), and that hard-soft grain interfaces where high GND(Geometrically Necessary Dislocation) densities develop are preferable.

An empirical microstructure-sensitive fatigue crack nucleation equation is given by

$$\dot{G} = \frac{\dot{U}\Delta V_s}{\Delta A_s} = \oint_C \frac{\xi\boldsymbol{\sigma}: d\boldsymbol{\varepsilon}^p}{\sqrt{\rho_{SSD} + \rho_{GND}}} \quad (23)$$

This criterion is developed from consideration of local slip activity and the local storage volume ΔV_s resulting from geometrically necessary ρ_{GND} and statistically stored dislocation ρ_{SSD} accumulation, defining a mean free distance induced from the plastic behaviour. The local stored energy per cycle considered is effectively derived from the point-wise crystal accumulated slip and the plastic energy associated with a stored fraction ξ.

Wilson et al [2019] investigated the microstructurally sensitive fatigue crack growth in four material systems with BCC, FCC and HCP crystallography through integrated crystal plasticity eXtended Finite Element (XFEM) modelling and experiment. The mechanistic drivers for crack path tortuosity and propagation rate have been investigated and crack propagation found to be controlled by crack tip stored energy and the crack direction by anisotropic crystallographic slip at the crack tip. Experimentally observed microstructurally-sensitive fatigue crack path tortuosities and growth rates in titanium alloy (Ti–6Al–4V), ferritic steel, nickel superalloy and zirconium alloy (zircaloy 4) have been shown to be captured, supporting the underpinning mechanistic arguments.
The crystal plasticity model is as follows:

$$\begin{gathered} F = F^e F^p \\ L^p = \dot{F}^p F^{p-1} = \sum_{i=1}^{N_s} (\dot{\gamma}^i n^i \otimes s^i) \\ \dot{\gamma}^i = \rho_m \nu b^2 \exp\,(\frac{\Delta F}{kT}) sinh\left[\frac{(\tau^i - \tau_c^i)\Delta V}{kT}\right] \\ \tau^i = \tau_{c0}^i + Gb\sqrt{\rho_{SSD} + \rho_{GND}} \\ \rho_{SSD} = \rho_{SSD} + \gamma_{st}\dot{p}dt \end{gathered} \tag{24}$$

where F is the deformation gradient and is assumed to be decomposable into two parts, elastic F^e and plastic F^p. L^p is the plastic velocity gradient, N_s is the total number of slip systems, $\dot{\gamma}^i$ is the slip rate on slip system i and n^i and s^i are the corresponding slip plane normal and slip direction respectively. ρ_m is the density of mobile dislocations, ν the frequency of attempts of dislocations to jump obstacle energy barriers, b the Burgers vector, ΔF the thermal activation energy, k the Boltzmann constant, T the temperature (295 K), τ^i and τ_c^i the resolved shear stress and critical resolved shear stress on slip system i respectively, and ΔV is the activation volume, γ_{st} is the hardening coefficient, $\dot{p}$ the rate of accumulated plastic strain, and dt the time increment. They used the empirical microstructure fatigue crack nucleation equation given by Eq (23).

Bandyopadhyay et al[2020] postulated that a microstructure-sensitive critical Plastic Strain Energy Density(SPSED) is the driving mechanism of fatigue crack initiation and is applicable to predict failure across several loading regimes. Crystal plasticity finite element simulations is used to compute the (local) SPSED at each material point within polycrystalline aggregates of a nickel-based superalloy. This critical plastic strain energy density is calibrated using experimental fatigue life data under fully reversed type loading at 1.2% applied strain range via the Bayesian inference method. Subsequently, the calibrated critical energy value is used to predict fatigue lives at eight strain ranges including strain ratios 1 and 0.05. A good agreement is observed between the experimental fatigue life and the lognormal mean of the predictions at eight strain ranges including strain ratios

Empirical fatigue life prediction model is given by

$$N_f^{\text{predict}}\left(\beta, W_{critical}^p\right) = \frac{W_{critical}^p - \omega_{N_s}^p(\beta, x^*)}{\Delta\omega_{N_s}^p(\beta, x^*)} + N_s(\beta) \tag{25}$$

Here, β is a set of empirical parameters which define the loading conditions, such as the applied strain range, strain ratio, temperature; $\omega_{N_s}^p(\beta, x^*)$, $\Delta\omega_{N_s}^p(\beta, x^*)$ and $N_s(\beta)$ come from the CPFE(crystal plasticity finite element) simulations; and $W_{critical}^p$ is the only model parameter which is to be calibrated from laboratory test data.

2.4.1 Other empirical models for metals

There are many other empirical models besides the JC type or modified GTN type that are well capable of modeling the mechanical behavior of metals under various strain rates.

Dondeti et al[2012] developed a rate-dependent homogenization-based continuum plasticity damage (HCPD) model for macroscopic analysis of ductile fracture in heterogeneous porous ductile materials such as dendritic cast aluminum alloys. The rate-dependent HCPD model follows the structure of an anisotropic Gurson–Tvergaard–Needleman elasto-porous-plasticity model for ductile materials. The model also incorporates an empirical rate-dependent void evolution criterion that is capable of effectively simulating the loss of load carrying capacity of heterogeneous materials resulting from inclusion cracking and void growth.

Darras et al[2013] presented a study on damage evolution in 5083 marine-grade aluminum alloy while deformed under different strain rates. Degradation in elastic moduli with the accumulation of plastic strain, and plastic strain energies at different strain rates were evaluated from the true stress–true strain curves. The energy-based empirical model predicts the damage evolution during deformation of 5083 Aluminum alloy at different strain rates.

Abed et al[2018] investigated the mechanical response of EN08 steel at quasi-static and dynamic strain rates. Through the stress-strain responses of EN08 steel, a strong

 doi:10.20944/preprints202102.0537.v1

dependency of the yield stress as well as the ultimate strength on the strain rate and temperature are recognized. Furthermore, the strain hardening is highly affected by the increasing temperature at all levels of strain rate. The microstructure of the steel is also examined at fracture by using SEM images to quantify the density of microdefects and define the damage evolution by using an energy-based empirical damage model.

$$\varphi = \left(\frac{U_p}{U_{PT}}\right)^{\alpha} \varphi_f \tag{26}$$

where φ is the damage at the point of interest during deformation, φ_f is the damage at fracture obtained by SEM images, U_p is the dissipated energy at the point of interest, U_{PT} is the total dissipated energy, and α is an empirical constant obtained by curve fitting to test data to determine the damage evolution trend throughout deformation.

Khoei et al[2013] simulated the crack growth in ductile materials under cyclic and dynamic loading with a damage–viscoplasticity model. The adaptive finite element method is used to model the discontinuity due to crack propagation. The ductile fracture assumptions and continuum damage mechanics are utilized to model the material rupture behavior. The rate-dependent constitutive equation was elaborated and the crack closure effect and combined hardening model were discussed. A viscoplastic model is modified to consider the damage effect as follows

$$\dot{\gamma} = \begin{cases} \frac{1}{\mu}[\left(\frac{q}{(1-D)\sigma_y(\bar{\varepsilon}^{vp})}\right)^{1/\Xi} - 1] & q \geq (1-D)\sigma_y(\bar{\varepsilon}^{vp}) \\ 0 & q \leq (1-D)\sigma_y(\bar{\varepsilon}^{vp}) \end{cases} \tag{27}$$

where μ and Ξ are empirical material constants, q is the von-Mises effective stress, σ_y is the material yield strength, $\bar{\varepsilon}^{vp}$ is the equivalent plastic strain, D is an empirical damage parameter.

Shojaei et al[2013] provided a model to capture low to high strain rate and ductile to brittle damage processes in dynamic problems of polycrystalline materials with different dynamic energy densities. Also, a novel fracture mechanics-based damage model is developed to describe the microcracking process. While micro-voiding models, such as Johnson void model (Johnson, 1981[111]), assume the hydrostatic part of the applied stress dominates the deformation mechanism, the developed microcracking model is suited for the problems with the dominant deviatoric stress.

Damage evolution: micro-void nucleation and growth rate are given by

$$\dot{D}^{(v)} = \dot{D}_N^{(v)} + \dot{D}_G^{(v)}$$

$$\dot{D}_N^{(v)} = \frac{m_1}{(1-D^{(v)})}\left[\exp\left(\frac{m_2|\Sigma - \sigma_N|}{kT} - 1\right)\right] \tag{28}$$

$$\dot{D}_G^{(v)} = \frac{1}{\eta} \exp\left(D^{(v)}\right) F\left(D^{(v)}, D_0^{(v)}\right) |\Sigma - \sigma_G|$$

where $\dot{D}^{(v)}$ is the total void volume fraction evolution rate, $\dot{D}_N^{(v)}$ is the rate of void nucleation, $\dot{D}_G^{(v)}$ is the rate of void growth. m_1 and m_2 are empirical curve fitting parameters, σ_N is hydrostatic threshold stress for microvoid nucleation, σ_G is for microvoid growth , Σ is the real damage stress, k is the Boltzmann constant, η is a viscosity parameter.

Chen et al[2014] introduced a reliability assessment model based on a local stress strain approach considering both low-cycle fatigue and high energy impact loads. The analysis of effects of an impact process on fatigue damage modifies the fatigue parameters and the Coffin–Manson equation for fatigue life to

$$\varepsilon_a = \frac{[1.75(\sigma_{b0} + p\dot{\varepsilon}^n) - \sigma_m](2N_f)^b}{E} + 0.5(\varepsilon_{f0} - q\dot{\varepsilon}^m)^{0.6}(2N_f)^c \qquad (29)$$

Eq. (29) is the modified empirical Coffin–Manson equation, in which p, n, q and m are the empirical curve fitting constants, σ_{b0} is the original static tensile strength, ε_{f0} the original static fracture ductility, ε_a is the plastic strain amplitude.

Carniel et al[2015] presented a one-dimensional finite element formulation for the transient analysis of geometrically nonlinear trusses associated with viscoelastic and viscoplastic materials including mechanical degradation. The proposed formulation aims at problems involving inertial loads and high strain rate deformations, and accounts for velocities, accelerations and rate-dependent effects. For high strain rates, where the damage evolution is abrupt, Lemaitre's damage model was able to represent satisfactorily the material degradation process.

Lemaitre's empirical damage evolution law is presented by

$$D = \frac{\delta A - \delta \bar{A}}{\delta A}$$

$$\dot{D} = \begin{cases} 0 & if \quad \bar{\varepsilon}^{vp} < \bar{\varepsilon}_D^{vp} \\ \frac{\dot{\gamma}}{1-D}\left(\frac{-Y}{r}\right)^S & if \quad \bar{\varepsilon}^{vp} \geq \bar{\varepsilon}_D^{vp} \end{cases} \text{ and } (-Y) = \frac{\sigma^2}{2E_0(1-D)^2} \qquad (30)$$

where δA is the total area of intersection of a given plane with a representative volume element, $\delta \bar{A}$ is the effective resisting area so that the damage variable can assume values $0 \leq D \leq 1$, r and S are empirical damage evolution parameters, $\bar{\varepsilon}_D^{vp}$ represents the damage threshold and $(-Y)$ is the damage strain energy density release rate. However, it is important to point that having plastic strain along as a criterion for damage potential as Eq (30) violates the second law of thermodynamics. Because if the load is applied million times below the critical strain rate, there can be no damage.

Shen et al[2015] presented a damage mechanics method applied successfully to assess fatigue life of notched specimens with plastic deformation at the notch tip. A damage-coupled elasto-plastic constitutive model is employed in which nonlinear kinematic hardening is considered. The accumulated damage is described by a stress-based damage model and a plastic strain-based damage model, which depend on the cyclic stress and accumulated plastic strain, respectively. A three-dimensional finite element implementation of these models is developed to predict the crack initiation life of notched specimens.

The damage evolution law in the plastic strain-based damage model is given by

$$\frac{dD_p}{dN} = \left[\frac{(\sigma_{max}^*)^2}{2ES(1-D)^2}\right]^m \Delta p \tag{31}$$

The damage evolution law in the stress-based damage model is given by

$$\frac{dD_e}{dN} = \left[1-(1-D)^{\beta+1}\right]^{1-a\langle\frac{A_{II}-\sigma_{l0}(1-3b_1\sigma_{H,mean})}{\sigma_u-\sigma_{eq,max}}\rangle}\left[\frac{A_{II}}{M_0(1-3b_2\sigma_{H,mean})(1-D)}\right]^\beta \tag{32}$$

Where σ_{max}^* is the maximum value of the damage equivalent stress over a loading cycle, E is the elastic modulus. The parameters S and m are determined from the experimentally determined curve of plastic strain versus number of cycles to failure. A_{II} and $\sigma_{H,mean}$ are the amplitude of the octahedral shear stress and the mean value of the hydrostatic stress in a loading cycle, respectively. The term $\sigma_{eq,max}$ is the maximum equivalent stress over a loading cycle, σ_{l0} is the fatigue limit at the fully reversed loading condition and σ_u is the ultimate tensile stress. The five parameters, a, M_0, β, b_1 and b_2, are determined by using plain fatigue tests of standard specimens.

Tang et al[2016] modified a damage model based on the Continuum Damage Mechanics (CDM) theory proposed by Kachanov[102] and later on developed by Lemaitre[103] to predict the formability of high strength steel sheets at elevated temperature by taking account the influence of the deformation temperature and strain rate. The material parameters of the modified Lemaitre-based damage evolution function were identified through an inverse analysis procedure based on tensile test data gained in a temperature range between 550ºC and 850ºC, at different strain rates.

Lemaitre's empirical damage potential is given by

$$F_Y = \frac{S_0}{(b+1)}\frac{1}{(1-D)}\left(\frac{-Y}{S_0}\right)^{b+1} \tag{33}$$

whereas the modified damage potential is given by

$$F_Y = \frac{S_0}{(b+1)(1-D)}\left(\frac{-Y}{S_0}\right)^{b+1} \left(\frac{1}{\bar{\varepsilon}^p}\right)^{\alpha} \tag{34}$$

In which S_0 and b are empirical materials parameters and are functions of the strain rate and temperature, Y is the damage strain energy density release rate, $\bar{\varepsilon}^p$ is the accumulated plastic strain, α is another empirical parameter obtained by curve fitting to test data.

Wu et al[2017] used a mechanism-based approach—the integrated creep-fatigue theory (ICFT)—to model low cycle fatigue behavior of 1.4848 cast austenitic steel over the temperature range from room temperature (RT) to 1173 K (900 °C) and the strain rate range from of 2x10^{-4} to 2x10^{-2} s^{-1}. The ICFT formulated the material's constitutive equation based on the physical strain decomposition into mechanism strains, and the associated damage accumulation consisting of crack nucleation and propagation in coalescence with internally distributed damage. Their empirical damage evolution equation is given by

$$D = 1 + \alpha\left[\left(\frac{\Delta\sigma_H}{\mu b}\right)^2 - \rho_0\right] + \beta\varepsilon_v \tag{35}$$

where $\Delta\sigma_H$ is the amplitude of cyclic hardening (maximum attainable peak stress minus the peak stress of the first cycle), ρ_0 is the dislocation density level below which there is no instantaneous crack nucleation, α the proportional constant for dislocation-nucleated cracks, β is the empirical proportional constant for creep damage, and ε_v is creep strain.

Phase field fracture models were applied to a number of problems in the field of fracture mechanics and were proven to yield reliable results even for complex crack problems. Mozaffari and Voyiadjis [2016] developed the framework of coupled nonlocal damage model through phase field method and viscoplasticity in continuum scale. It is shown that the proposed non-local gradient type damage model through the phase field method can be coupled to a viscoplastic model to capture the inelastic behavior of the rate dependent material.

The empirical damage evolution law incorporating the viscoplastic deformation is given below

$$\frac{\partial\phi}{\partial t} = -M\big(2(1-\phi)\bar{E}_{ijkl}(\bar{\varepsilon}_{ij} - \bar{\varepsilon}^{vp}_{ij})(\bar{\varepsilon}_{kl} - \bar{\varepsilon}^{vp}_{kl}) - 4W_p\phi(1-\phi)(2-\phi) - \epsilon_\eta^2\nabla^2\phi\big) \tag{36}$$

where $\bar{E}_{ijkl}$ is effective stiffness tensor, $\bar{\varepsilon}_{ij}$ is effective strain tensor, $\bar{\varepsilon}^{vp}_{ij}$ is effective viscoplastic strain tensors, in undamaged configuration. M is an empirical scalar function to map the state of stress between the damaged configuration and effective undamaged configuration for the case of isotropic damage, $\bar{\sigma}_{ij} = M(\phi)\sigma_{ij}$. W_p is the material constant with energy dimensions and it needs to be emphasized that the value of this constant contains dissipation during the whole process of damage through elastic and viscoplastic deformations. The constant ϵ_η^2 is considered in the form $\epsilon_\eta^2 = W_p l_d^2$ to separate the effect of energy type constant (W_p) and length unit, in which l_d corresponds to the length scale due to damage.

Furthermore, Badnava at al[2017] proposed a phase field viscoplastic model to model the influence of the loading rate on the ductile fracture, as one of the main causes of metallic alloys' failure. The effects of the phase field are incorporated in the Peric's viscoplastic model[106]; Schreiber et al[2020] utilize the framework of phase field modeling for fracture in order to handle fatigue crack growth.

Dynamic brittle fracture and shear banding are typical failure modes in metals under high strain rate loading. Chu et al[2019] developed a unified phase field damage model to simulate both brittle tensile fracture and shear banding. The model can capture the above two failure modes' transition naturally by allowing the critical energy release rate to vary with the stress triaxiality to distinguish the material failure properties of tensile fracture and shear banding. The failure energy excluding the plastic dissipation in the fracture process zone before damage evolution is defined to model the ductile failure more physically. Besides, the degradation function of the yield stress is introduced which not only provides a damage softening mechanism for the ductile failure but also ensures a proper simulation of the brittle fracture.
The failure energy density is given by

$$\psi_d(d) = \frac{G_{cd}}{2l}[d^2 + l^2|\nabla d^2|] \ , \ G_{cd} = G_c - G_{c0} \tag{37}$$

where l is am empirical length scale parameter associated with the regulation of sharp discontinuities, the empirical damage parameter d with $d = 0$ defining the intact state and $d = 1$ defining the fully damaged state of the material. G_{cd} is the equivalent critical energy release rate corresponding to the evolution of the internal discontinuous boundary, G_c is the critical energy release rate obtained by experiments, and $G_{c0} < G_c$ is the failure parameter to consider the energy release before damage initiation in the fracture process zone (FPZ). The evolution equation for the phase field is given by

$$\begin{gathered} \left[\frac{G_c}{2l} - \frac{w_0}{1-\chi}\right][d^2 - l^2|\nabla d^2|] = (1-d)\mathcal{H} \\ \mathcal{H}(\boldsymbol{x}, t) = \max_{s \in [0,t]} \langle \psi_{e0}^{+}(\boldsymbol{x}, s) + \psi_{p0}(\boldsymbol{x}, s) - w_0(\boldsymbol{x}, s) \rangle \end{gathered} \tag{38}$$

For a homogeneous stretch problem of ideal elasto-plastic material

$$d = \frac{\mathcal{H}}{\mathcal{H} + G_c/2l}$$
$$\mathcal{H} = \left\langle \int \sigma_0 d\varepsilon - w_0 \right\rangle \tag{39}$$

where χ is empirical fraction of plastic work converted to heat , ψ_{e0}^{+} is compression part of the inherent elastic strain energy density, ψ_{p0} is the inherent plastic stored energy density, w_0 is an empirical energy density threshold, which can be understood as the stored deformation energy requiring for the microstructural evolution, such as recrystallization, before the damage initiation. ε and σ_0 are one-dimensional strain and inherent stress, respectively.

2.4.2 Empirical models for non-metallic materials at high strain rates

Besides metals, there are many studies focusing on the fatigue modeling of laminates or composites. Morinière et al[2014] published a review of modeling of impact damage and dynamics in fiber-metal laminates.

Composite materials

Zhang et al[2014] investigated the mechanical behaviors of a 2D plain woven composites(2DPWC) under high strain rate compression along the thickness direction experimentally and modeled with FEM at microstructural level. The failure morphologies of 2DPWCs were found to be different depending on the strain rate of the loading.
They proposed the following empirical criterion for damage initiation:

$$\omega_D = \int \frac{d\bar{\varepsilon}^{pl}}{\bar{\varepsilon}_D^{pl}(\eta, \dot{\bar{\varepsilon}}_D^{pl})} = 1 \tag{40}$$

And their empirical damage evolution law is given by

$$\dot{D} = \frac{\dot{\bar{u}}^{pl}}{\dot{\bar{u}}_f^{pl}} \tag{41}$$

where $\eta = -p/q$ is the stress triaxiality, p is the pressure stress, q is the Mises equivalent stress, $\dot{\bar{\varepsilon}}_D^{pl}$ Is the equivalent plastic strain rate and $\dot{\bar{u}}^{pl}$ is the effective displacement rate. $\dot{\bar{u}}_f^{pl}$ is the maximum value of the effective displacement at the point of failure

Alemi-Ardakani et al[2014] presented two empirical models for fast simulation of out-of-plane impact response of fiber reinforced polymer composites. The model considers four main effects: (a) strain rate dependency of the mechanical properties, (b) difference between tensile and flexural bending responses, (c) delamination, and (d) the geometry of fixture (clamping conditions). To show the application of the two approaches, a glass fiber reinforced polypropylene composite was subjected to impact at 200J and was simulated in Abaqus/Explicit. The built-in Hashin's empirical damage criterion was used for progressive damage of the material.

Hashin's failure criterion

Fiber tension ($\hat{\sigma}_{11} \geq 0$) Matrix tension($\hat{\sigma}_{22} \geq 0$)

$$F_f^t = \left(\frac{\hat{\sigma}_{11}}{X^T}\right)^2 + \alpha\left(\frac{\hat{\tau}_{12}}{S^L}\right)^2 \qquad F_m^t = \left(\frac{\hat{\sigma}_{22}}{Y^T}\right)^2 + \alpha\left(\frac{\hat{\tau}_{12}}{S^L}\right)^2 \tag{42}$$

Fiber compression ($\hat{\sigma}_{11} \leq 0$) Matrix compression ($\hat{\sigma}_{22} \leq 0$)

$$F_f^c = \left(\frac{\hat{\sigma}_{11}}{X^C}\right)^2 \qquad F_m^c = \left(\frac{\hat{\sigma}_{22}}{2S^T}\right)^2 + \left[\left(\frac{Y^C}{2S^T}\right)^2 - 1\right]\frac{\hat{\sigma}_{22}}{Y^C} + \left(\frac{\hat{\tau}_{12}}{S^L}\right)^2 \tag{43}$$

where X^T, X^C, Y^T, Y^C, S^L, S^T are the longitudinal tensile strength, longitudinal compressive strength, transverse tensile strength, transverse compressive strength, longitudinal shear strength, and transverse shear strength, respectively. $\hat{\sigma}_{11}$, $\hat{\sigma}_{22}$, $\hat{\tau}_{12}$ refer to the in-plane normal and shear stresses (the 1-direction is aligned with fibers direction). The empirical coefficient α defines the contribution of the shear stress to the fiber tensile failure initiation.

Chen and Morozov[2016] developed and validated an elasto-viscoplastic damage model that accounts for the strain rate-dependent plastic response and the progressive post-failure behavior of composite materials. The proposed model is suitable for progressive failure analysis of composite materials and structures subjected to loadings at various strain rates. A strain rate-dependent yield criterion is adopted; whereas the standard Kuhn–Tucker conditions for plastic loading and unloading is utilized. Also, the plastic consistency condition for strain rate-dependent material is satisfied.

The empirical exponential damage evolution law adopted for each damage variable is given as

$$d_I = 1 - \frac{1}{r_I}\exp\left(A_I(1 - r_I)\right) \;, \quad I = \{1t, 1c, 2t, 2c, 6\} \tag{44}$$

where r_I is an empirical damage threshold corresponding to each failure mechanism, A_I is an empirical parameter that defines the exponential softening law. r_I is an empirical parameter that controls the size of the expanding damage surface and depends on the loading history, the initial value of r_I is 1; subscripts 1 and 2 represent the fibre and transverse directions of the unidirectional ply; subscripts t and c denote tension and compression. The damage variable d6 represents the damage effects on the shear stiffness due to matrix fracture caused by a combined action of transverse and shear stresses.

Park et al[2015] focused on rate-dependent damage modeling for polymeric composite materials with the rate-dependent constitutive model using a multi-scale approach. Phenomenologically, the nonlinear response of a composite under the in-plane shear loading condition is due to the viscoplasticity of a matrix and the damage behavior of composite materials. In case of dynamic loading, the strain-rate effects the damage behavior of composite materials, as well as the behavior of the matrix. The enhanced micromechanical model which improves the in-plane shear behavior, is used for analyzing the rate-dependent behaviors of the fiber and matrix constituents. The rate-dependent elastic damage model based on orthotropic continuum damage mechanics theory at the micromechanical level is applied to improve the accuracy of the model.

The empirical damage evolution laws are expressed follows

$$d_2 = \frac{\langle Y - Y_2^0 \rangle_+}{Y_2^c} \quad d_6 = \frac{\langle Y - Y_6^0 \rangle_+}{Y_6^c} \tag{45}$$

where Y is an empirical damage variable, Y_2^0, Y_2^c, Y_6^0 and Y_6^c are empirical damage constants representing the transverse damage initiation, transversely critical damage, in-plane shear damage initiation, and in-plane shear critical damage, respectively.

Seman et al[2019] presented a multi-scale finite element modelling scheme to analyze the damage behaviors of Kenaf fiber reinforced composite materials subjected to high strain rate compressions. The proposed modelling framework includes a micro-scale structure model with periodic boundary conditions for homogenizing the heterogeneous fiber/resin system into a unit cell, and a meso-scale model with established constitutive relationship for the constituents integrated with failure criterion to account for the stiffness degradation and subsequent element removal. For the composite they proposed the following empirical evolution functions

The ductile criteria for damage initiation is met when:

And the shear criteria for damage initiation is met when::

$$\omega_D = \int \frac{d\bar{\varepsilon}^{pl}}{\bar{\varepsilon}_D^{pl}(\eta, \dot{\bar{\varepsilon}}_D^{pl})} = 1 \qquad \omega_s = \int \frac{d\bar{\varepsilon}^{pl}}{\bar{\varepsilon}_s^{pl}(\eta, \dot{\bar{\varepsilon}}^{pl})} = 1 \tag{46}$$

In which

$$\bar{\varepsilon}_D^{pl}\left(\eta, \dot{\bar{\varepsilon}}_D^{pl}\right) = \frac{\varepsilon_T^+ sinh[k_0(\eta^- - \eta)] + \varepsilon_T^- sinh[k_0(\eta - \eta^+)]}{sinh[k_0(\eta^- - \eta^+)]}$$

$$\bar{\varepsilon}_S^{pl}(\theta_s, \dot{\bar{\varepsilon}}^{pl}) = \frac{\varepsilon_s^+ sinh[f(\theta_s - \theta_s^-)] + \varepsilon_T^- sinh[k_0(\theta_s^+ - \theta_s)]}{sinh[k_0(\theta_s^+ - \theta_s^-)]} \tag{47}$$

where ε_T^+ and ε_T^- correspond to the equivalent plastic strain at ductile damage initiation for uniaxial tensile and uniaxial compressive deformation, respectively, $\eta^+ = 1/3$ and $\eta^- = -1/3$ are the stress triaxiality in uniaxial tensile and compressive deformation state, k_0 is an empirical parameter, $\theta_s = (1 - k_s\eta)/\phi$, $\phi = \tau_{max}\sigma_{eq}$, ε_s^+ and ε_s^- correspond to the equivalent plastic strain at shear damage initiation for uniaxial tensile and compressive deformation, respectively. The parameters θ_s^+ and θ_s^- correspond to the values of θ_s at $\eta = \eta^+$ and, $\eta = \eta^-$ respectively. k_s and f are curve fitting empirical parameters. Two different dynamic failure models, both the ductile and shear failure models are described for the matrix whereas Hashin's failure criterion was used for the fibre to predict the mechanical behavior of the Kenaf composite under distinct high strain rate loading.

Alabdullah and Ghoniem[2020] developed an empirical damage model and validated with experimental data for the non-linear mechanical behavior of SiC/SiC composite materials in nuclear applications. Cyclic thermal and mechanical loading associated with neutron irradiation leads to wide-spread and progressive micro-cracking that leads to loss of thermal conductivity and further enhancement of thermo-mechanical damage. A model for wide-spread micro-cracking is developed within the thermodynamic framework of continuum damage mechanics. Evolution equations for damage parameters that describe the growth of continuum damage are developed empirically, where the curve fitting parameters are obtained from experiments. The model novelty is in coupling mechanical, thermal, and irradiation damage through a consistent thermodynamic framework, including loss of thermal conductivity due to the evolution of mechanically induced micro-cracks.

The total damage is a result of mechanical loading, neutron radiation, and temperature gradients.

$$d_k^t = d_k^m + d_k^{irr} + d_k^{\nabla T} \tag{48}$$

$$d_k^m = d_k^{m0}\left\{1 - exp\left(-\left(\frac{\sqrt{y_{kmax}^{*m}} - \sqrt{y_{0k}^m}}{\sqrt{y_{bk}^m}}\right)^{c_k}\right)\right\} \text{ for } k = 1 - 6 \tag{49}$$

$$d_k^{irr} = d_k^{irr0}\left[1 - c_{0k}^{irr}(T)\tanh\left(-\left(\sqrt{y_{k_{max}}^{irr}} - \sqrt{y_{0k}^{irr}}\right)^{c_{1k}^{irr}}\right)\right]$$

Where empirical parameters $y_{k_{max}}^{*m}$, y_{0k}^{m}, y_{bk}^{m}, c_k, d_k^{m0} are the maximum effective thermodynamic force obtained during the loading history (in case there is unloading), initial damage threshold, thermodynamic normalizing force constant, shaping parameter, and maximum damage obtained (amplitude), respectively. $y_{k_{max}}^{irr}$, y_{0k}^{m}, c_k^{irr} are the maximum thermodynamic force obtained during the radiation history, initial damage threshold, shaping parameter. The parameter d_k^{irr0} is a material constant related to the damage associated with volumetric swelling (micro voids and/or small dislocation loops).

Laminates

Sitnikova et al[2014] developed a 3-D nonlinear finite element models to simulate blast failure of fibre metal laminates. In their work, an empirical damage evolution law is incorporated into the composite constitutive behavior to obtain the blast response of FML(Fibre-metal laminate) panels. The proposed formulation is applicable to composites with a plane weave architecture, as well as with possible through thickness damage.

The empirical damage evolution in the model is as follows:

$$\begin{aligned}
\dot{d}_{1t} &= \alpha_1\left(\left(\frac{\hat{\sigma}_{11}}{\sigma_{1t}^r}\right)^2 - 1\right) && \text{If } f_{1t} \geq 0 \ , \ \Delta\varepsilon_{11} > 0 \\
\dot{d}_{1c} &= \alpha_1\left(\left(\frac{\hat{\sigma}_{11}}{\sigma_{1t}^r}\right)^2 - 1\right) && \text{If } f_{1c} \geq 0 \ , \ \Delta\varepsilon_{11} < 0 \\
\dot{d}_{2t} &= \alpha_1\left(\left(\frac{\hat{\sigma}_{11}}{\sigma_{1t}^r}\right)^2 - 1\right) && \text{If } f_{2t} \geq 0 \ , \ \Delta\varepsilon_{22} > 0 \\
\dot{d}_{2c} &= \alpha_1\left(\left(\frac{\hat{\sigma}_{11}}{\sigma_{1t}^r}\right)^2 - 1\right) && \text{If } f_{2c} \geq 0 \ , \ \Delta\varepsilon_{22} < 0 \\
\dot{d}_{3c} &= \alpha_2\left(\left(\frac{\hat{\sigma}_{11}}{\sigma_{1t}^r}\right)^2 - 1\right) && \text{If } f_{3c} \geq 0 \ , \ \Delta\varepsilon_{33} < 0 \\
\dot{d}_{12} &= \alpha_2\left(\left(\frac{\hat{\sigma}_{11}}{\sigma_{1t}^r}\right)^2 - 1\right) && \text{If } f_{12} \geq 0
\end{aligned} \tag{50}$$

where the d_i are the damage variables, namely, d_1 and d_2 correspond to the failure in warp and weft fibre directions, respectively, d_{3c} describes through the-thickness composite crushing failure, and d_{12} refers to the in-plane shear failure. The subscripts "t" and "c" denote tensile and compressive failure. $\hat{\sigma}_{ij}$ are effective stresses, σ_{ij}^{r} are material strengths. Empirical coefficients α_1 and α_2 in the above equation govern the rate of growth of damage.

Cement and asphalt mortar

Fu et al[2017] investigated the dynamic behavior of cement and asphalt mortar experimentally under impact loading using a Split Hopkinson Pressure Bar(SHPB). The strain rate effects on the compressive strength, elastic modulus, peak strain and specific energy absorption were obtained. The results showed that the compressive strength and specific energy absorption increased with increasing strain rate. A statistical continuous damage constitutive model involving the strain rate for CA(cement and asphalt) mortar was proposed.

The empirical damage evolution equation is given by

$$D = \left[1 - \exp\left[-(R_i)^{\gamma}\left(\frac{\varepsilon}{\alpha}\right)^{\beta}\right]\right] \tag{51}$$

where ε is the total strain of CA mortar, R_i is any strain rate under impact loading, γ is an empirical strain rate sensitivity index of the damage variable, α is an empirical scale parameter related to the strength; β is the empirical morphological parameter of the Weibull distribution.

2.5 Models using irreversible entropy as a metric with an empirical evolution function

Basaran and Yan[1998] proposed using entropy as a damage metric. Chandaroy and Basaran[1999[a], 1999[b]] used energy dissipated during thermal cycling in a microelectronic solder joint to model fatigue life.

Naderi et al [2010] proposed a thermodynamic approach for the characterization of material degradation, which uses the entropy generated during the entire life of the specimens undergoing fatigue tests. Results show that the cumulative entropy generation is constant at the time of failure and is independent of geometry, load and frequency. Moreover, it is shown that the fatigue fracture entropy, FFE is a material property. That is, materials with different properties, such as stainless steel and Al have a different cumulative entropy generation at the fracture point. Figure 1 and 2 shows the FFE of Al 6061-T6 and SS 304 for different loads and frequencies. The results presented in Figure 1 and 2 demonstrate the validity of the constant entropy gain at failure for Al and SS specimens. The results reveal that the necessary and sufficient condition for final fracture of Al 6061-T6 corresponds to the entropy gain of $4MJm^{-3}$ K^{-1}, regardless of the test frequency, thickness of the specimen and the stress state. For SS 304 specimens, this condition corresponds to an entropy gain of about 60MJ m^{-3} K^{-1}.

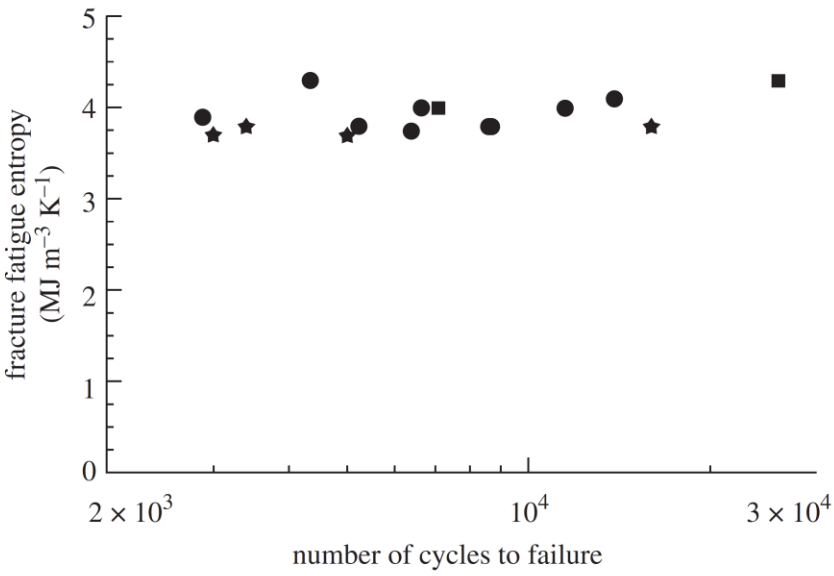

Figure 1. Experimental fracture fatigue entropy versus the number of cycles to failure for tension-compression, bending and torsional fatigue tests of Al 6061-T6 at frequency 10 Hz.

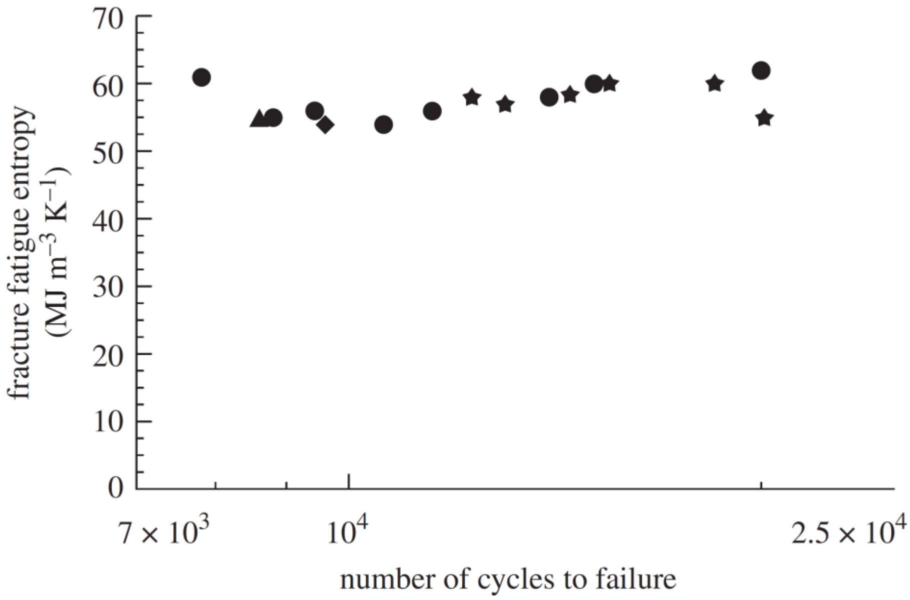

Figure 2. Experimental fracture fatigue entropy versus the number of cycles to failure for bending and torsional fatigue tests of SS 304 for different loads and frequencies.

Naderi and Khonsari[2010] presented an experimental approach to fatigue damage in metals based on thermodynamic theory of irreversible process. Fatigue damage is an irreversible progression of cyclic plastic strain energy that reaches its critical value at the onset of fracture. In this work, irreversible cyclic plastic energy in terms of entropy generation is utilized to experimentally determine the degradation of different specimens subjected to low cyclic bending, tension-compression, and torsional fatigue The entropy generation equation is given by

$$s_g = \int_0^{t_f} (W_p/T)dt \tag{52}$$

where s_g is the total entropy generation at the onset of fracture, W_p is the cyclic plastic energy, T is the absolute temperature . The cyclic plastic energy determined by Morrow's cyclic plastic energy dissipation formula is given below

$$W_p = 2\sigma_f'\varepsilon_f'\left(\frac{1-n'}{1+n'}\right)(2N_f)^{1+b+c} \tag{53}$$

where n' is the cyclic strain hardening exponent, ε_f' is the fatigue ductility coefficient, σ_f' denotes the fatigue strength coefficient, N_f is the final number of cycles when failure occurs, b is fatigue strength exponent and c is fatigue ductility exponent. Damage evolution is given by

$$D_c = D_0 + Bln(1 - s_{ic}/s_g) \tag{54}$$

where D_0 is the initial damage, s_{ic} is the critical value of entropy generation at the time when temperature starts to rise just after the steady-state phase, and B is a curve fitting parameter.

Applying the same entropy generation equation, Amiri and Khonsari [2012] assessed degradation in processes involving metal fatigue. It is shown that empirical fatigue models such as Miner's rule, Coffin-Manson equation, and Paris law can be deduced from thermodynamic consideration. In the work by Naderi and Khonsari [37], they again presented a methodology for real-time monitoring of fatigue life in machinery components that utilizes the accumulation of entropy to assess the severity of degradation associated with fatigue. Using this concept, a prototype called the fatigue monitoring unit that automatically shuts down the machine prior to the onset of fatigue fracture entropy based on a user-specified factor of safety is developed. The method is applicable to variable loading and does not require the specification of the loading history or loading sequence. The results of a series of laboratory fatigue tests pertaining to Al 6061-T6 and SS 304 specimens, which show the utility of the approach and its suitability for implementation in the field, are provided. Similar work was also done by Teng et al [2020] for normalized SAE1045 steel.

$$\dot{s} = W_p/T - \boldsymbol{J_q} \cdot \boldsymbol{grad\, T}/T^2 \;\; ; \;\; W_p = AN_f^{\alpha}; \;\; \alpha = b + c \tag{55}$$

Preprints (www.preprints.org) | NOT PEER-REVIEWED | Posted: 24 February 2021 doi:10.20944/preprints202102.0537.v1

$$A = 2^{2+b+c}\sigma_f'\varepsilon_f'\left(\frac{c-b}{c+b}\right)(N_f)^{b+c} \ ; \ s_f = \int_0^{t_f}(W_p/T)dt$$

where $\dot{s}$ represents the entropy production rate ($\dot{s} \geq 0$), $\boldsymbol{J_q}$ the heat flux, T the surface temperature, W_p the cyclic plastic energy per unit volume, N_f is the final number of cycles when failure occurs, b and c are curve fitting parameters, b is fatigue strength exponent and c is fatigue ductility exponent, ε_f' is the fatigue ductility coefficient, σ_f' denotes the fatigue strength coefficient.

Liakat and Khonsari[2015] utilized the concept of thermodynamic entropy generation in a degradation process to study the high cycle fatigue of medium carbon steel 1018. The evolutions of the plastic strain energy and temperature are discussed and utilized to calculate the entropy accumulation. It is shown that the accumulation of entropy generation in the high cycle fatigue of the material, beginning with a pristine specimen and ending at fatigue fracture is nearly constant within the experimental and loading conditions considered. The concept of tallying entropy is useful for the prediction of the fatigue life evolution of a material undergoing cyclic loading.

$$s = \int_0^{N_f}(\Delta W_p/T)dN - \int_0^{N_f}\left(\frac{k}{T^2}grad\ T\right)dN \tag{56}$$

Ontiveros et al[2016] examined a set of experimental results of AA7075-T651 to determine applicability of the thermodynamic entropy generation as an index of fatigue crack initiation. Entropy accumulation is calculated from hysteresis energy and temperature rise. An increasing trend of entropy accumulation with the number of cycle to failure is observed on macroscale measurements. Results also determine that the entropy generations from the samples under the same operating conditions are similar as the crack grows. Scanning electron microscope analysis is performed on the fractured surfaces to observe the fatigue striations, and persistent slip bands are observed employing an optical microscope. A discussion is presented regarding the length scales on which crack initiation occurs and entropy calculation is made.

Guo et al[2018] introduced a new intrinsic dissipation model for high-cycle fatigue life prediction of metallic materials. A general constitutive model with internal state variables, in accordance with the thermodynamic principles, is firstly formulated to describe the thermo-mechanical response of metallic materials under high-cycle fatigue loading. The model formulation considers two types of micro-mechanisms, i.e. the recoverable microstructure motion inducing anelasticity and the unrecoverable microstructure motion inducing damage. The intrinsic dissipation model is then derived taking into account two critical stress amplitudes related to the corresponding microstructure. Finally, a fatigue life prediction model is obtained by taking the intrinsic dissipation part induced solely by the unrecoverable microstructure motion as a fatigue damage indicator. Failure criterion is estimated by the concept of energy dissipation threshold.

The quantitative assessment of cumulative damage caused by unrecoverable microstructure motion is given as

$$D = \frac{N k_d \sigma_a^p}{E_c f}[H(\sigma_a - \sigma_{c2})] \tag{57}$$

where N is the cycle number, E_c is the energy dissipation threshold for fatigue failure which can be identified using the proposed intrinsic dissipation model with experimental data, f is the frequency, σ_a is the stress amplitude , σ_{c2} is the critical stress amplitude for the onset of the unrecoverable deformation mechanism., which is considered as a material fatigue limit $\sigma_{c2} = \sigma_0$ in the proposed model, k_d and p are experimental curve fitting parameters. $H(\bullet)$ denotes the Heaviside step function.

Ribeiro et al [2019] studied low cycle fatigue for an Al-2024 specimen in a classical thermodynamics' framework. From the thermomechanical formulation, authors estimate the fatigue fracture entropy based on temperature measurements (where emissivity uncertainty is shown to have a small influence on the FFE estimation). Estimation of this quantity based on a mechanical empirical model is also possible. The various estimations seem to converge towards the fact that a constant fatigue fracture entropy (FFE) exists, where the Park and Nelson empirical model (model which relates the cyclic deformation work to the number of cycles endured by the material) produces a value in accordance with the experimental determination procedure.

The fatigue fracture entropy is given by

$$FFE_{TB} \cong \int_0^{t_f} \frac{-2ka_y(t)}{T_m(t)} dt + \int_0^{t_f} \rho C \left(\frac{\dot{T}_m(t)}{T_m(t)}\right) dt + \int_0^{t_f} \frac{[h_G \frac{S_{conv}}{V_{spe}}(T_m(t) - T_0)]}{T_m(t)} dt \tag{58}$$

where FFE_{TB} is the total entropy generated during the fatigue tests obtained from thermal balance. In Eq. (32), the first term is the contribution from heat conduction, the second term is from heat accumulation, third term is from convection and radiation when we consider them as heat source. T_m is the mean temperature, k is the thermal conductivity, a_y is a parameter obtained by parabolic curve fitting to the temperature profile, ρ is the density, C is the heat capacity, h_G is the global heat transfer coefficient, S_{conv} is exchange surface, V_{spe} is the specimen volume.

Roslinda Idris et al[2019] assessed the fatigue crack growth rate for dual-phase steel under spectrum loading based on entropy generation. According to the second law of thermodynamics, fatigue crack growth is related to entropy gain because of its irreversibility. In this work, the temperature evolution and crack length were simultaneously measured during fatigue crack growth tests until failure to ensure the validity of the assessment. Results indicated a significant correlation between fatigue crack growth rate and entropy. This relationship is the basis in developing a model that can determine the characteristics of fatigue crack growth rate, particularly under spectrum loading. Predictive results showed that the proposed model can accurately predict the fatigue crack growth rate under a spectrum loading in all cases.

The number of cycles for crack length to propagate from distance a_j to a_{j+2}, can be obtained as

$$\Delta N_{j+2} = \int_{a_j}^{a_{j+2}} [y]da$$
$$= \frac{a_j(r^2-1)}{6r}[y_j r(2-r) + y_{j+1}(r+1)^2 + y_{j+2}(2r-1)] \tag{59}$$

where j is the number sequence, y_j is the difference between the numbers of cycles for crack length interval, r is the interval between the crack length and y represents dN/da.

Osara and Bryant [2019] developed a Degradation-Entropy-Generation (DEG) methodology based on original work by Basaran and Yan [1998] and Basaran and Nie [2004] for system and process characterization and failure analysis on metal low-cycle fatigue. The method combines the first and second laws of thermodynamics with the Helmholtz free energy, then applies the result to the degradation-entropy generation theorem to relate a desired fatigue measure—stress, strain, cycles or time to failure—to the loads, materials and environmental conditions (including temperature and heat) via the irreversible entropies generated by the dissipative processes that degrade the fatigued material. The formulations are then verified with fatigue data from the literature, for a steel shaft under bending and torsion, entropies are given by

$$S'_{w} = \int_0^t \frac{\sigma\dot{\varepsilon}}{T}dt = N_{\Delta t}\sum_1^m \left\{\frac{\sigma_m}{T_m}[\varepsilon_{em} + \varepsilon_{pm}\left(\frac{1-n'}{1+n'}\right)]\right\}$$
$$S'_{\mu T} = \int_0^t -(\rho c \ln(T) + \frac{\alpha}{\kappa_T}\varepsilon)\frac{\dot{T}}{T}dt = -\sum_1^m \left(\rho c \ln(T_m) + \frac{\alpha}{\kappa_T}\varepsilon_m\right)\frac{\Delta T_m}{T_m} \tag{60}$$

where indices 1, 2, 3, … , m correspond to times $t_1, t_2, t_3, \ldots, t_m$, $N_{\Delta t}$ is the total number of cycles within sampling time increment, n' is the cyclic strain hardening coefficient , ε_{em}, ε_{pm}, σ_m, T_m are elastic and plastic strain, stress, absolute temperature at t_m, respectively, ρ is the density, c is the heat capacity, κ_T is isothermal loadability, α is thermal expansion coefficient.

Sun et al [2019] proposed a copula entropy approach, which is a combination of the copula function and information entropy theory, to measure the dependence among different degradation processes. The copula function was employed to identify the complex dependence structure of performance features, and information entropy theory was used to quantify the degree of dependence. The copula entropy is given by

$$H_c(u_1,u_2,\dots,u_d) = -\int_0^1 \dots \int_0^1 c(u_1,u_2,\dots,u_d)\ln\big(c(u_1,u_2,\dots,u_d)\big)\,du_1,\dots,du_d \tag{61}$$

where $c(u_1,u_2,\dots,u_d)$ is the probability density function of the copula function; $u_i = F_i(x_i) = P(x_i \le X_i)$, $i = 1,2,\dots,d$, represents the marginal distribution function of random variables.

The probability density function, $p_i(x)$, of the ith performance feature degradation increment is calculated as

$$p_i(\Delta x) = \frac{1}{mh}\sum_{t=1}^{T} K(\frac{\Delta x - \Delta X_t}{h})$$
$$K\left(\frac{\Delta x - \Delta X_t}{h}\right) = \frac{1}{\sqrt{2\pi}}\exp\left(-\frac{(\Delta x - \Delta X)^2}{2h^2}\right) \tag{62}$$

where t is the time interval; T is the width of the time interval; h is the width of the form smooth parameter, ΔX is the increment of degradation data, and $K()$ is a kernel function, which is a standard Gaussian distribution.

Yun and Modarres [2019] proposed the entropic damage indicators for metallic material fatigue processes obtained from three associated energy dissipation sources. In this study, three entropic-based metrics are examined and demonstrated for application to fatigue damage. Experimental data on energy dissipations associated with fatigue damage, in the forms of mechanical, thermal, and acoustic emission (AE) energies are collected. These data are estimated and correlated the corresponding entropy generations with the observed fatigue damages in metallic materials.

The classical thermodynamic entropy equation is given by

$$\dot{S} = \frac{1}{T^2}J_q \cdot \nabla T - \sum_k J_k\left(\nabla\frac{\mu_k}{T}\right) + \frac{1}{T}\tau\colon\dot{\varepsilon}_p + \frac{1}{T}\sum_j v_j A_j + \frac{1}{T}\sum_m c_m J_m(-\nabla\psi) \tag{63}$$

The AE information (Shannon) entropy is given by

$$S = -\sum_k p(x_i)\log\, p(x_i) \tag{64}$$

The entropy from the definition of statistical mechanics is given by

$$\Delta S_{tot} = k_b \ln \left(\frac{\pi_f(+W)}{\pi_r(-W)} \right) \tag{65}$$

where J_q is the thermodynamic flux due to heat conduction, J_k is the thermodynamic flux due to diffusion, μ_k is the chemical potential, τ is the mechanical stress, ε_p is the plastic strain, v_j is the chemical reaction rate, A_j is the chemical affinity, c_m is the coupling constant, J_m is the thermodynamic flux due to the external field, and ψ is the potential of the external field. $p(x_i)$ is a corresponding discrete histogram for processed digitized data, $\pi_f(+W)$ and $\pi_r(-W)$ in the fatigue damage process are interpreted as the forward and reverse work distributions over many load cycles, respectively.

Young and Subbarayan [2009] proposed using the cumulative distribution functions derived from maximum entropy formalisms, utilizing thermodynamic entropy as a measure of damage to fit the low-cycle fatigue data of metals. The thermodynamic entropy is measured from hysteresis loops of cyclic tension–compression fatigue tests on aluminum 2024-T351. The plastic dissipation per cyclic reversal is estimated from Ramberg–Osgood constitutive model fits to the hysteresis loops and correlated to experimentally measured average damage per reversal. The developed damage models are shown to more accurately and consistently describe fatigue life than several alternative damage models, including the Weibull distribution function and the Coffin–Manson relation. The formalism is founded on treating the failure process as a consequence of the increase in the entropy of the material due to plastic deformation. This argument leads to using inelastic dissipation as the independent variable for predicting low-cycle fatigue damage, rather than the more commonly used plastic strain.

The Ramberg–Osgood plasticity model for stress–strain loops are

$$\Delta\epsilon_p = \left(\frac{\Delta\sigma}{K}\right)^{\frac{1}{n}}, \ \Delta\epsilon_{total} = \frac{\Delta\sigma}{E} + \left(\frac{\Delta\sigma}{K}\right)^{\frac{1}{n}} \tag{66}$$

where $\Delta\epsilon_p$ is Plastic strain range, $\Delta\sigma$ is Stress range, K is Ramberg–Osgood strength parameter and $1/n$ is Ramberg–Osgood exponent. The Damage per reversal is proposed as a function of inelastic dissipation per reversal with power law fit

$$D_{rev} = f\left(\frac{W_f}{2N_f}\right) \tag{67}$$

And the inelastic dissipation for a monotonic test is

$$\frac{W_f}{2N_f} = \frac{1}{1+n}\sigma_f \epsilon_f \tag{68}$$

where σ_f is the true fracture stress, ϵ_f is the true fracture strain, $2N_f$ is the Total reversals to failure, W_f is the Total inelastic dissipation (per unit volume) to failure

Wang and Yao [2019] proposed an entropy-based failure prediction model for the creep and fatigue of metallic materials based on the Boltzmann probabilistic entropy theory and continuum damage mechanics. The relationship between entropy increase rate during creep process and normalized creep failure time is developed and compared with the experimental results. A model based on empirical formula for the evolution law of entropy increase rate is developed to predict the change of creep strain during the damage process.

The entropy-based creep strain prediction equation is given as

$$p = \frac{p_{cr}}{\exp\left(\exp\left(\ln\left(\ln\left(\frac{p_{cr}}{p_{th}}\right)\right)\right)\right)} - B\left[\ln\left(\ln\left(\frac{t_f}{f}\right)\right) - \ln\left(\ln\left(\frac{t_f}{t_{th}}\right)\right)\right] \tag{69}$$

$$B = \frac{Am_s}{N_0 k_0 \alpha}$$

where p_{th} is the initial value of cumulative plasticity in the microstructure of material, which represents the value at the beginning of creep damage accumulation; p_{cr} is the threshold value of cumulative plastic variable when creep failure occurs. The corresponding creep time when $p = p_{th}$ and $p = p_{cr}$ are t_{th} and t_f , respectively. The parameter B is related to the applied stress, temperature, and material properties.

Sosnovskiy and Sherbakov [2019] substantiated and formulated the main principles of the physical discipline-mechanothermodynamics (MTD) that unites Newtonian mechanics and thermodynamics. Its principles are based on using entropy as a bridge between mechanics and thermodynamics. The analysis of more than 600 experimental results allowed for determining a unified mechanothermodynamical function of limiting states (critical according to damageability) of polymers and metals. They are also known as fatigue fracture entropy states.

The generalized expressions for entropy in the MTD system consisting of a liquid (gas) medium of volume V and a solid of volume V_ψ is given by

$$S = \int_V \rho s_T dV + \int_{V_\psi} \sum_l \rho s_l \, dV_\psi + \int_{u_\Sigma^{eff} \geq 0} \rho s_{TF} dV_\psi = \int_V \frac{1}{T} \sigma_{ij} \varepsilon_{ij} dV +$$

$$\int_V \frac{1}{T} \rho dV + \int_V \frac{1}{T} \rho \sum_k \mu_k n_k dV + \int_{V_\psi} \frac{1}{T} \sum_k \rho[(1-a_k)u_k] \, dV_\psi \tag{70}$$

$$+ \int_{u_\Sigma^{eff} \geq 0} \rho \psi_u^{eff} dV_\psi$$

where s_{TF} is the specific tribo-fatigue entropy, u_0 is the limiting density of the internal energy treated as the initial activation energy of the disintegration process, u_Σ^{eff} is the total effective energy of the system, ψ_u^{eff} is a dimensionless parameter of local energy damageability, $\psi_u^{eff} = u_\Sigma^{eff}/u_0$. q is the heat flux, μ is the chemical potential, n_k is the number of mols per unit mass, a_k are experimentally found coefficients.

3. Physics based evolution functions: unified mechanics theory

The models presented in the previous sections that predict material degradation evolution are based on empirical curve fitting of the experimental data. Most do not satisfy the 2nd law of thermodynamics. Because according to the 2nd law of thermodynamics only entropy can be a damage or degradation criteria, not stress or strain or displacement.

Unified mechanics theory[70][90], on the other hand, is a purely physics-based approach that doesn't need any experimental data curve fitting for degradation evolution function. It is obtained by combining the universal laws of motion of Newton and the first and second laws of thermodynamics directly at the ab-initio level. The second and third law of unified mechanics are given by, [90]

The second law $$(1-\phi)F\,dt = d(mv) \tag{71}$$

The third law $$F_{12} = \frac{d[\frac{1}{2}K_{21}{u_{21}}^2(1-\phi)]}{du_{21}} \tag{72}$$

In unified mechanics the material is treated as a thermodynamic system. As a result, governing partial differential equations of any system automatically include energy loss, entropy generation and degradation of the system. A damage evolution is calculated along the Thermodynamic State Index axis, TSI, is given by [90]

$$\phi = \phi_{cr}\left[1-\exp\left(\frac{-\Delta s m_s}{R}\right)\right] \tag{73}$$

ϕ_{cr} is the critical value of TSI, Δs is the change in entropy, m_s is the molar mass and R is the gas constant. Equation (73) is the normalized form of the second law of thermodynamics. When a material in ground (reference) state, it is assumed to be free of any possible defects, i.e. "damage", it can be assumed that "damage" in material is equal to zero. Therefore, TSI will be $\phi = 0$. However, ϕ does not have to be zero initially. In final stage, material reaches a critical state, such that entropy is maximum. At this stage, entropy production rate will become zero. Therefore, TSI will be $\phi = 1$. Thermodynamic State Index ϕ is an additional axis of the unified mechanics theory that maps the entropy generation rate between zero and one. It predicts the lifespan of

 doi:10.20944/preprints202102.0537.v1

any closed system without curve fitting an empirical model to a test data just using the thermodynamic fundamental equation of the material/system. Figure 3 shows the coordinate system in unified mechanics theory. It is important to emphasize that in the new coordinate system derivative of displacement with respect to entropy is not zero because TSI is a linearly independent axis.

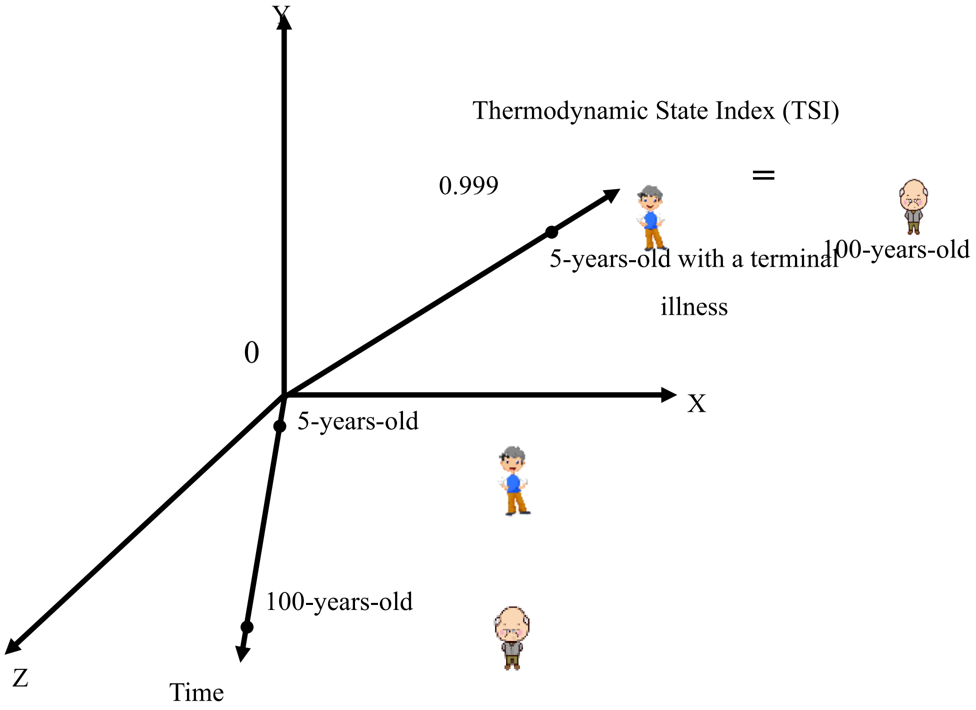

Figure 3. Coordinate system in unified mechanics theory

In unified mechanics theory, in addition to nodal displacements, the entropy generation rate is also necessary to relate microstructural changes in the material with spatial and temporal coordinates. In the following, some studies that adopted this concept and has been experimentally and mathematically validated will be listed and some will be discussed.

Unified Mechanics Theory (UMT) was used for fatigue life prediction under thermo-mechanical loading, [115]-[135]. Life predictions were validated by experiments. Noushad et al [2020] showed that the unified mechanics theory can be used to predict fatigue life of Ti-6Al-4V alloys based on fundamental equation of the material. Similarly, Egner et al [2020] analyzed the low cycle fatigue behavior of P91 steel using the exponential damage evolution equation derived in unified mechanics theory. First, experimental tests are performed to recognize different aspects of material behavior. Then an appropriate constitutive model is developed within the framework of thermodynamics of irreversible processes with internal state variables. Two different approaches to fatigue damage modeling are applied comparatively to describe the final

stage of material cyclic softening. The material parameters are identified, and the model is validated based on the available experimental data.
The fundamental equation of the steel under low cycle fatigue is given by:

$$\Delta s = \int_{t_0}^{t} \frac{\sigma_{ij}\varepsilon_{ij}^{p}}{\theta\rho} dt + \int_{t_0}^{t} \frac{k^{\theta}|grad\theta|^{2}}{\theta^{2}\rho} dt + \int_{t_0}^{t} \frac{r^{\theta}}{\theta} dt \tag{74}$$

and the exponential damage evolution equation is derived as follows:

$$\phi = \left[1 - e^{\frac{-\Delta s}{N_0 k}}\right] \tag{75}$$

In comparison with the classical ductile damage model(Chaboche-Lemaitre ductile damage model [103][104]) in which the process of micro-cracks and micro-voids development starts when the accumulated plastic strain reaches a certain threshold value, the entropy-based model includes damage developing from the very beginning of the loading scheme. Egner et al [2020] concluded that unified mechanics theory gives better fatigue predictions.

Unified Mechanics Theory (UMT) was also used for fatigue under electrical-thermal-mechanical loading,[136]-[150]. A model was implemented into finite element procedure for prediction of nanoelectronics solder joint's time to failure under high current density. Nonlinear viscoplastic time-dependent nature of the material and current crowding effects are considered in the formulation.
The fundamental equation of the nanoelectronics solder joint is given by:

$$\Delta s = \int_{t_0}^{t} \left(\frac{1}{T^2} c|\mathrm{Grad}(T)^2| + \frac{C_v D_v}{kT^2} (Z^* e\rho \boldsymbol{j} - f\Omega\nabla\sigma + \frac{Q\nabla \mathrm{T}}{T} + \frac{kT}{C}\nabla C)^2 + \frac{1}{T}\boldsymbol{\sigma}: \varepsilon_p \right) dt \tag{76}$$

where D_v is effective vacancy diffusivity, C_{v0} is the equilibrium vacancy concentration in the absence of a stress field, C_v is instantaneous atomic vacancy concentration, c is normalized vacancy concentration $c = C_v/C_{v0}$, Z^* is vacancy effective charge number, e is electronic charge of an electron, k is Boltzmann's constant, T is absolute temperature, ρ is metal resistivity, $\vec{j}$ is current density vector, f is atomic vacancy relaxation ratio, Ω is atomic volume, $\sigma_{spherical} = \mathrm{trace}(\sigma_{ij})/3$, ε_p is the plastic strain rate tensor, Q^* is heat of transport, the isothermal heat transmitted by the moving atom in the process of jumping a lattice site. Δs is the entropy production, N_0 is Avogadro's constant.

Besides metals, UMT can also be used for fatigue life prediction in particle filled composites. These models were verified experimentally[151]-[156].

5. Summary

This review article includes some recently developed degradation, damage evolution or fatigue life prediction models for different strain rates. For the empirical evolution function models, various modified GTN models, modified JC models, microplasticity models, phase-field models, and models based on irreversible continuum thermodynamics are included. For the physics-based evolution models, models based on unified mechanics are reviewed.

REFERENCES

[1] Ožbolt, J. & Tonkovic, Zdenko & Lackovic, Luka. (2015). Microplane Model for Steel and Application on Static and Dynamic Fracture. Journal of Engineering Mechanics. 142. 04015086. 10.1061/(ASCE)EM.1943-7889.0000993.

[2] Ted Sjöberg, Jörgen Kajberg, Mats Oldenburg, Fracture behaviour of Alloy 718 at high strain rates, elevated temperatures, and various stress triaxialities, Engineering Fracture Mechanics, Volume 178, 2017, Pages 231-242, ISSN 0013-7944, https://doi.org/10.1016/j.engfracmech.2017.04.036.

[3] S.S. Jafari, G.H. Majzoobi, E. Khademi, M. Kashfi, Development of a new technique for measuring damage accumulation at high strain rates, Engineering Fracture Mechanics, Volume 209, 2019, Pages 162-172, ISSN 0013-7944, https://doi.org/10.1016/j.engfracmech.2019.01.020.

[4] Acharyya, S., Dhar, S. A complete GTN model for prediction of ductile failure of pipe. J Mater Sci 43, 1897–1909 (2008). https://doi.org/10.1007/s10853-007-2369-0

[5] Bugang Teng, Weinian Wang, Yongchao Xu, Ductile fracture prediction in aluminium alloy 5A06 sheet forming based on GTN damage model, Engineering Fracture Mechanics, Volume 186, 2017, Pages 242-254, ISSN 0013-7944, https://doi.org/10.1016/j.engfracmech.2017.10.014.

[6] Gui Li, Saisai Cui, Meso-mechanics and damage evolution of AA5182-O aluminum alloy sheet Based on the GTN model, Engineering Fracture Mechanics, Volume 235, 2020, 107162, ISSN 0013-7944, https://doi.org/10.1016/j.engfracmech.2020.107162.

[7] Liang Xue, Constitutive modeling of void shearing effect in ductile fracture of porous materials, Engineering Fracture Mechanics, Volume 75, Issue 11, 2008, Pages 3343-3366, ISSN 0013-7944, https://doi.org/10.1016/j.engfracmech.2007.07.022.

[8] Youbin Chen, Chunyu Zhang, Christophe Varé, An extended GTN model for indentation-induced damage, Computational Materials Science, Volume 128, 2017, Pages 229-235, ISSN 0927-0256, https://doi.org/10.1016/j.commatsci.2016.11.043.

[9] Cheng Jin, Jitai Niu, Shiyu He, Chengbin Fu, Modeling thermal cycling induced micro-damage in aluminum welds: An extension of Gurson void nucleation model, Computational Materials Science, Volume 43, Issue 4, 2008, Pages 1165-1171, ISSN 0927-0256, https://doi.org/10.1016/j.commatsci.2008.03.008.

[10] T. Linse, G. Hütter, M. Kuna, Simulation of crack propagation using a gradient-enriched ductile damage model based on dilatational strain, Engineering Fracture Mechanics, Volume 95, 2012, Pages 13-28, ISSN 0013-7944, https://doi.org/10.1016/j.engfracmech.2012.07.004.

[11] K. Nahshon, J.W. Hutchinson, Modification of the Gurson Model for shear failure, European Journal of Mechanics - A/Solids, Volume 27, Issue 1, 2008, Pages 1-17, ISSN 0997-7538, https://doi.org/10.1016/j.euromechsol.2007.08.002.

[12] Xu, F. & Zhao, S. & Han, X.. (2013). Use of a modified Gurson model for the failure behaviour of the clinched joint on Al6061 sheet. Fatigue & Fracture of Engineering Materials & Structures. 37. 10.1111/ffe.12118.

[13] Shakir Gatea, Hengan Ou, Bin Lu, Graham McCartney, Modelling of ductile fracture in single point incremental forming using a modified GTN model, Engineering Fracture Mechanics, Volume 186, 2017, Pages 59-79, ISSN 0013-7944, https://doi.org/10.1016/j.engfracmech.2017.09.021.

[14] L. Malcher, F.M. Andrade Pires, J.M.A. César de Sá, An extended GTN model for ductile fracture under high and low stress triaxiality, International Journal of Plasticity, Volume 54, 2014, Pages 193-228, ISSN 0749-6419, https://doi.org/10.1016/j.ijplas.2013.08.015.

[15] Shen Wang, Zhanghua Chen, Chaofang Dong, Tearing failure of ultra-thin sheet-metal involving size effect in blanking process: Analysis based on modified GTN model, International Journal of Mechanical Sciences, Volume 133, 2017, Pages 288-302, ISSN 0020-7403, https://doi.org/10.1016/j.ijmecsci.2017.08.028.

[16] He Wu, Wenchen Xu, Debin Shan, Bo Cheng Jin, An extended GTN model for low stress triaxiality and application in spinning forming, Journal of Materials Processing Technology, Volume 263, 2019, Pages 112-128, ISSN 0924-0136, https://doi.org/10.1016/j.jmatprotec.2018.07.032.

[17] Markus Bambach, Muhammad Imran, Extended Gurson–Tvergaard–Needleman model for damage modeling and control in hot forming, CIRP Annals, Volume 68, Issue 1, 2019, Pages 249-252, ISSN 0007-8506, https://doi.org/10.1016/j.cirp.2019.04.063.

[18] Zeping Wang, Zhiqiang Hu, Kun Liu, Gang Chen, Application of a material model based on the Johnson-Cook and Gurson-Tvergaard-Needleman model in ship collision and grounding simulations, Ocean Engineering, Volume 205, 2020, 106768, ISSN 0029-8018, https://doi.org/10.1016/j.oceaneng.2019.106768.

[19] li, Fang & Qi, Xue & Xiang, Dan. (2014). Finite Element Modeling of Crack Generation in Laser Shock Peening Processed Airfoils. Advances in Materials Science and Engineering. 2014. 1-10. 10.1155/2014/812705.

[20] Jeunechamps, P.-P & Ponthot, Jean-Philippe. (2013). An efficient 3D implicit approach for the thermomechanical simulation of elastic-viscoplastic materials submitted to high strain rate and damage. International Journal for Numerical Methods in Engineering. 94. 920-960. 10.1002/nme.4489.

[21] Hyun-Suk Nam, Jin-Ho Je, Jae-Jun Han, Yun-Jae Kim, Investigation of Crack Tip Stress and Strain Fields at Crack Initiation of A106 Gr. B Carbon Steels under High Strain Rates, Procedia Materials Science, Volume 3, 2014, Pages 764-771, ISSN 2211-8128, https://doi.org/10.1016/j.mspro.2014.06.125.

[22] H.-S. Nam, J.-Y. Jeon, J.-S. Kim, J.-W. Kim, Y.-J. Kim, A Strain Rate Dependent Computational Model of Ductile Damage for C(T) Specimen, Procedia Engineering, Volume 130, 2015, Pages 861-867, ISSN 1877-7058, https://doi.org/10.1016/j.proeng.2015.12.212.

[23] G. Khatibi, A. Betzwar Kotas, M. Lederer, Effect of aging on mechanical properties of high temperature Pb-rich solder joints, Microelectronics Reliability, Volume 85, 2018, Pages 1-11, ISSN 0026-2714, https://doi.org/10.1016/j.microrel.2018.03.009.

[24] Chen, H. et al. "Experimental Investigation into Corrosion Effect on Mechanical Properties of High Strength Steel Bars under Dynamic Loadings." International Journal of Corrosion 2018 (2018): 1-12.

[25] Guang Chen, Chengzu Ren, Lianpeng Lu, Zhihong Ke, Xuda Qin, Xiang Ge, Determination of ductile damage behaviors of high strain rate compression deformation for Ti-6Al-4V alloy using experimental-numerical combined approach, Engineering Fracture Mechanics, Volume 200, 2018, Pages 499-520, ISSN 0013-7944, https://doi.org/10.1016/j.engfracmech.2018.08.020.

[26] Jianjun Wang, Xueyao Hu, Kangbo Yuan, Weihua Meng, Penghui Li, Impact resistance prediction of superalloy honeycomb using modified Johnson–Cook constitutive model and fracture criterion, International Journal of Impact Engineering, Volume 131, 2019, Pages 66-77, ISSN 0734-743X, https://doi.org/10.1016/j.ijimpeng.2019.05.001.

[27] Qian Zhu, Chao Zhang, Jose L. Curiel-Sosa, Tinh Quoc Bui, Xiaojing Xu, Finite element simulation of damage in fiber metal laminates under high velocity impact by projectiles with different shapes, Composite Structures, Volume 214, 2019, Pages 73-82, ISSN 0263-8223, https://doi.org/10.1016/j.compstruct.2019.02.009.

[28] Wang, Xuchen & Hassani, Mostafa. (2020). Ultra-High Strain Rate Constitutive Modeling of Pure Titanium Using Particle Impact Test. Journal of Applied Mechanics. 87. 10.1115/1.4047290.

[29] Long-hui Zhang, Antonio Pellegrino, Nik Petrinic, Dynamic necking of a near α titanium alloy at high strain rates: Experiments and modelling, Defense Technology, 2020, ISSN 2214-9147, https://doi.org/10.1016/j.dt.2020.07.002.

[30] T. Chiyatan, V. Uthaisangsuk, Mechanical and fracture behavior of high strength steels under high strain rate deformation: Experiments and modelling, Materials Science and Engineering: A, Volume 779, 2020, 139125, ISSN 0921-5093, https://doi.org/10.1016/j.msea.2020.139125.

[31] M. Naderi, M.M. Khonsari, An experimental approach to low-cycle fatigue damage based on

thermodynamic entropy, International Journal of Solids and Structures, Volume 47, Issue 6, 2010, Pages 875-880, ISSN 0020-7683, https://doi.org/10.1016/j.ijsolstr.2009.12.005.

[32] Amiri, Mehdi & Khonsari, M.. (2012). On the Role of Entropy Generation in Processes Involving Fatigue. Entropy. 14. 24-31. 10.3390/e14010024.

[33] M. Liakat, M.M. Khonsari, On the anelasticity and fatigue fracture entropy in high-cycle metal fatigue, Materials & Design, Volume 82,2015,Pages 18-27,ISSN 0264-1275,https://doi.org/10.1016/j.matdes.2015.04.034.

[34] Naderi, Mehdi & Amiri, Mehdi & Khonsari, M.. (2010). On the thermodynamic entropy of fatigue fracture. Proceedings of The Royal Society A Mathematical Physical and Engineering Sciences. 466. 10.1098/rspa.2009.0348.

[35] Ontiveros, V & Amiri, Mehdi & Kahirdeh, Ali & Modarres, Mohammad. (2016). Thermodynamic Entropy Generation in the Course of the Fatigue Crack Initiation. Fatigue & Fracture of Engineering Materials & Structures. 40. 10.1111/ffe.12506.

[36] Patrick Ribeiro, Johann Petit, Laurent Gallimard, Experimental determination of entropy and exergy in low cycle fatigue, International Journal of Fatigue, Volume 136, 2020, 105333, ISSN 0142-1123, https://doi.org/10.1016/j.ijfatigue.2019.105333.

[37] Naderi, Mehdi & Khonsari, M.. (2010). Real-time fatigue life monitoring based on thermodynamic entropy. Structural Health Monitoring-an International Journal - STRUCT HEALTH MONIT. 9. 10.1177/1475921710373295.

[38] Idris, R.; Abdullah, S.; Thamburaja, P.; Omar, M.Z. Prediction of Fatigue Crack Growth Rate Based on Entropy Generation. *Entropy* **2020**, *22*, 9.

[39] Osara, J.A.; Bryant, M.D. Thermodynamics of Fatigue: Degradation-Entropy Generation Methodology for System and Process Characterization and Failure Analysis. *Entropy* **2019**, *21*, 685.

[40] Dondeti, Piyush & Paquet, Daniel & Ghosh, Somnath. (2012). A rate-dependent homogenization based continuum plasticity-damage (HCPD) model for dendritic cast aluminum alloys. Engineering Fracture Mechanics. 89. 75–97. 10.1016/j.engfracmech.2012.04.018.

[41] Darras, Basil & Abed, Farid & Pervaiz, Salman & Abdul-Latif, Akrum. (2013). Analysis of Damage in 5083 Aluminum Alloy Deformed at Different Strain Rates. Materials Science and Engineering A. 568. 143-149. 10.1016/j.msea.2013.01.039.

[42] A.R. Khoei, M. Eghbalian, H. Azadi, H. Saffar, Numerical simulation of ductile crack growth under cyclic and dynamic loading with a damage–viscoplasticity model,Engineering Fracture Mechanics, Volume 99, 2013, Pages 169-190, ISSN 0013-7944, https://doi.org/10.1016/j.engfracmech.2012.12.009.

[43] Hongxia Chen, Yunxia Chen, Zhou Yang, Coupling damage and reliability model of low-cycle fatigue and high energy impact based on the local stress–strain approach, Chinese Journal of Aeronautics, Volume 27, Issue 4, 2014,Pages 846-855, ISSN 1000-9361, https://doi.org/10.1016/j.cja.2014.03.008.

[44] T.A. Carniel, P.A. Muñoz-Rojas, M. Vaz, A viscoelastic viscoplastic constitutive model including mechanical degradation: Uniaxial transient finite element formulation at finite strains and application to space truss structures, Applied Mathematical Modelling, Volume 39, Issues 5–6, 2015, Pages 1725-1739, ISSN 0307-904X, https://doi.org/10.1016/j.apm.2014.09.036.

[45] B.T. Tang, S. Bruschi, A. Ghiotti, P.F. Bariani, An improved damage evolution model to predict fracture of steel sheet at elevated temperature, Journal of Materials Processing Technology, Volume 228, 2016, Pages 76-87, ISSN 0924-0136, https://doi.org/10.1016/j.jmatprotec.2015.08.007.

[46] Wu, X., Quan, G. & Sloss, C. Mechanism-Based Modeling for Low Cycle Fatigue of Cast Austenitic Steel. *Metal Mater Trans A* **48,** 4058–4071 (2017). https://doi.org/10.1007/s11661-017-4160-4

[47] Long, X., He, X. & Yao, Y. An improved unified creep-plasticity model for SnAgCu solder under a wide range of strain rates. *J Mater Sci* **52,** 6120–6137 (2017). https://doi.org/10.1007/s10853-017-0851-x

[48] Abed, Farid & Abdul-Latif, Akrum & Yehia, Ayatollah. (2018). Experimental Study on the Mechanical Behavior of EN08 Steet al Different Temperatures and Strain Rates.

[49] Zhenglin Chen, Zhidan Sun, Benoît Panicaud, Investigation of ductile damage during surface mechanical attrition treatment for TWIP steels using a dislocation density based viscoplasticity and damage models, Mechanics of Materials, Volume 129, 2019, Pages 279-289, ISSN 0167-6636, https://doi.org/10.1016/j.mechmat.2018.12.009.

[50] F.D. Morinière, R.C. Alderliesten, R. Benedictus, Modelling of impact damage and dynamics in fibre-metal laminates – A review, International Journal of Impact Engineering, Volume 67, 2014, Pages 27-38, ISSN 0734-743X, https://doi.org/10.1016/j.ijimpeng.2014.01.004.

[51] Amir Shojaei, George Z. Voyiadjis, P.J. Tan, Viscoplastic constitutive theory for brittle to ductile damage in polycrystalline materials under dynamic loading, International Journal of Plasticity, Volume 48, 2013, Pages 125-151, ISSN 0749-6419, https://doi.org/10.1016/j.ijplas.2013.02.009.

[52] Zhang, Fa & Wu, Liwei & Wan, Yumin & Rotich, Gideon & Gu, Bohong & Sun, Baozhong. (2014). Numerical modeling of the mechanical response of basalt plain woven composites under high strain rate compression. Journal of Reinforced Plastics and Composites. 33. 1087-1104. 10.1177/0731684413503190.

[53] Jendli, Zouhaier & Walrick, Jean-Christophe & Bocquet, Michel & Fitoussi, Joseph. (2014). Strain rate effects on the mechanical behavior of carbon-thermoplastic matrix woven composites. 16th European Conference on Composite Materials, ECCM 2014.

[54] Alemi-Ardakani, Mohammad & Milani, A & Yannacopoulos, Spiro. (2014). On Complexities of Impact Simulation of Fiber Reinforced Polymer Composites: A Simplified Modeling Framework. TheScientificWorldJournal. 2014. 382525. 10.1155/2014/382525.

[55] Jing-Fen Chen, Evgeny V. Morozov, A consistency elasto-viscoplastic damage model for progressive failure analysis of composite laminates subjected to various strain rate loadings,

Composite Structures, Volume 148, 2016, Pages 224-235, ISSN 0263-8223, https://doi.org/10.1016/j.compstruct.2016.03.049.

[56] Ill Kyung Park, Kook Jin Park, Seung Jo Kim, Rate-dependent damage model for polymeric composites under in-plane shear dynamic loading, Computational Materials Science, Volume 96, Part B, 2015, Pages 506-519, ISSN 0927-0256, https://doi.org/10.1016/j.commatsci.2014.04.067.

[57] Pradeep Lall, Di Zhang, Vikas Yadav, David Locker, High strain rate constitutive behavior of SAC105 and SAC305 leadfree solder during operation at high temperature, Microelectronics Reliability, Volume 62, 2016, Pages 4-17, ISSN 0026-2714, https://doi.org/10.1016/j.microrel.2016.03.014.

[58] E. Sitnikova, Z.W. Guan, G.K. Schleyer, W.J. Cantwell, Modelling of perforation failure in fibre metal laminates subjected to high impulsive blast loading, International Journal of Solids and Structures, Volume 51, Issue 18, 2014, Pages 3135-3146, ISSN 0020-7683, https://doi.org/10.1016/j.ijsolstr.2014.05.010.

[59] Qiang Fu, Youjun Xie, Guangcheng Long, Ditao Niu, Hao Song, Xiguang Liu, Impact characterization and modelling of cement and asphalt mortar based on SHPB experiments, International Journal of Impact Engineering, Volume 106, 2017, Pages 44-52, ISSN 0734-743X, https://doi.org/10.1016/j.ijimpeng.2017.03.009.

[60] Amir Nourani, Saeed Akbari, Gholamhossein Farrahi, Jan K. Spelt, Strain-rate dependent influence of adherend stiffness on fracture load prediction of BGA solder joints, Engineering Fracture Mechanics, Volume 186, 2017, Pages 119-133, ISSN 0013-7944, https://doi.org/10.1016/j.engfracmech.2017.09.027.

[61] M. Shirinbayan, J. Fitoussi, M. Bocquet, F. Meraghni, B. Surowiec, A. Tcharkhtchi, Multi-scale experimental investigation of the viscous nature of damage in Advanced Sheet Molding Compound (A-SMC) submitted to high strain rates, Composites Part B: Engineering, Volume 115, 2017, Pages 3-13, ISSN 1359-8368, https://doi.org/10.1016/j.compositesb.2016.10.061.

[62] Hao Jiang, Fan Jiang, Dianyin Hu, Rongqiao Wang, Jian Lu, Bo Li, Numerical modeling of compressive failure mechanisms in ceramic materials at high strain rates, Computer Methods in Applied Mechanics and Engineering, Volume 347, 2019, Pages 806-826, ISSN 0045-7825, https://doi.org/10.1016/j.cma.2019.01.006.

[63] Sareh Aiman Hilmi Abu Seman, Roslan Ahmad, Hazizan Md Akil, Meso-scale modelling and failure analysis of kenaf fiber reinforced composites under high strain rate compression loading, Composites Part B: Engineering, Volume 163, 2019, Pages 403-412, ISSN 1359-8368, https://doi.org/10.1016/j.compositesb.2019.01.037.

[64] Basaran, C.; Yan, C.Y. A thermodynamic framework for damage mechanics of solder joints. *J. Electron. Packag. Trans. ASME* **1998**, *120*, 379–384.

[65] Cemal Basaran, Minghui Lin, Damage mechanics of electromigration induced failure, Mechanics of Materials, Volume 40, Issues 1–2, 2008, Pages 66-79, ISSN 0167-6636, https://doi.org/10.1016/j.mechmat.2007.06.006.

[66] Li, Shidong & Mohd, Fazly & Basaran, Cemal. (2008). Simulating Damage Mechanics of Electromigration and Thermomigration. Simulation. 84. 391-401. 10.1177/0037549708094856.

[67] Yao, Wei & Basaran, Cemal. (2012). Electromigration analysis of solder joints under ac load: A mean time to failure model. Journal of Applied Physics. 111. 10.1063/1.3693532.

[68] Wei Yao, Cemal Basaran, Electromigration damage mechanics of lead-free solder joints under pulsed DC: A computational model, Computational Materials Science, Volume 71, 2013, Pages 76-88, ISSN 0927-0256, https://doi.org/10.1016/j.commatsci.2013.01.016.

[69] Władysław Egner, Piotr Sulich, Stanisław Mroziński, Halina Egner, Modelling thermo-mechanical cyclic behavior of P91 steel, International Journal of Plasticity, Volume 135, 2020, 102820, ISSN 0749-6419, https://doi.org/10.1016/j.ijplas.2020.102820.

[70] Mankarathodi, Noushad & Kumar, Aman & Lakshmana Rao, Chebolu & Basaran, Cemal. (2020). Low Cycle Fatigue Life Prediction Using Unified Mechanics Theory in Ti-6Al-4V Alloys. Entropy. 22. 24. 10.3390/e22010024.

[71] Xin Yang, Xiangguo Zeng, Jian Wang, Jiabin Wang, Fang Wang, Jun Ding, Atomic-scale modeling of the void nucleation, growth, and coalescence in Al at high strain rates, Mechanics of Materials, Volume 135, 2019, Pages 98-113, ISSN 0167-6636, https://doi.org/10.1016/j.mechmat.2019.05.005.

[72] V.V.C. Wan, M.A. Cuddihy, J. Jiang, D.W. MacLachlan, F.P.E. Dunne, An HR-EBSD and computational crystal plasticity investigation of microstructural stress distributions and fatigue hotspots in polycrystalline copper, Acta Materialia, Volume 115, 2016, Pages 45-57, ISSN 1359-6454, https://doi.org/10.1016/j.actamat.2016.05.033.

[73] Bo Chen, Jun Jiang, Fionn P.E. Dunne, Is stored energy density the primary meso-scale mechanistic driver for fatigue crack nucleation?, International Journal of Plasticity, Volume 101, 2018, Pages 213-229, ISSN 0749-6419, https://doi.org/10.1016/j.ijplas.2017.11.005.

[74] David Wilson, Weifeng Wan, Fionn P.E. Dunne, Microstructurally-sensitive fatigue crack growth in HCP, BCC and FCC polycrystals, Journal of the Mechanics and Physics of Solids, Volume 126, 2019, Pages 204-225, ISSN 0022-5096, https://doi.org/10.1016/j.jmps.2019.02.012.

[75] Bandyopadhyay, Ritwik & Veerappan, Prithivirajan & Peralta, Alonso & Sangid, Michael. (2020). Microstructure-sensitive critical plastic strain energy density criterion for fatigue life prediction across various loading regimes. Proceedings of the Royal Society A: Mathematical, Physical and Engineering Sciences. 476. 20190766. 10.1098/rspa.2019.0766.

[76] Alabdullah, Mohammad & Ghoniem, Nasr. (2020). A thermodynamics-based damage model for the non-linear mechanical behavior of SiC/SiC ceramic matrix composites in irradiation and thermal environments. International Journal of Damage Mechanics. 29. 105678952094157. 10.1177/1056789520941574.

[77] R. W. Rohde.1973; Metallurgical Effects at High Strain Rates 1st Edition, ISBN 978-1-4615-8696-8

[78] T.Z. Blazynski .1987; Materials at High Strain Rates 1st Edition, ISBN 978-1-85166-067-4

[79] Bischoff, P.H., Perry, S.H. Compressive behaviour of concrete at high strain rates. *Materials and Structures* **24,** 425–450 (1991). https://doi.org/10.1007/BF02472016

[80] M. Nabil Bassim, N. Panic, High strain rate effects on the strain of alloy steels, Journal of Materials Processing Technology, Volumes 92–93, 1999, Pages 481-485, ISSN 0924-0136, https://doi.org/10.1016/S0924-0136(99)00248-4.

[81] A.G. Odeshi, S. Al-ameeri, M.N. Bassim, Effect of high strain rate on plastic deformation of a low alloy steel subjected to ballistic impact, Journal of Materials Processing Technology, Volumes 162–163, 2005, Pages 385-391, ISSN 0924-0136, https://doi.org/10.1016/j.jmatprotec.2005.02.157.

[82] C.Y. Gao, L.C. Zhang, Constitutive modelling of plasticity of fcc metals under extremely high strain rates, International Journal of Plasticity, Volumes 32–33, 2012, Pages 121-133, ISSN 0749-6419, https://doi.org/10.1016/j.ijplas.2011.12.001.

[83] K. Naresh, K. Shankar, B.S. Rao, R. Velmurugan, Effect of high strain rate on glass/carbon/hybrid fiber reinforced epoxy laminated composites, Composites Part B: Engineering, Volume 100, 2016, Pages 125-135, ISSN 1359-8368, https://doi.org/10.1016/j.compositesb.2016.06.007.

[84] Voyiadjis, G & Palazotto, Anthony & Gao, X.-L. (2020). Modeling of metallic materials at high strain rates with continuum damage mechanics. 10.1115/1.1495522.

[85] Gurson, A.L. Plastic Flow and Fracture Behavior of Ductile Materials Incorporating Void Nucleation, Growth and Interaction. Ph.D. Thesis, Brown University, Providence, RI, USA, 1975.

[86] Boyer, J.C.; Vidal-Salle, E.; Staub, C. A shear stress dependent ductile damage models .Int. J. Mater. Process. Technol.2003,121, 87–93.

[87] Weck, A.; Seguarado, J.; Lorca, J.L.; Wilkinson, D. Numerical simulations of void linkage in model materials using a nonlocal ductile damage approximation. Int. J. Fract.2007,148, 205–219

[88] Johnson, G.R.; Cook, W.H. Fracture characteristics of three metals subjected to various strains, strain rates, temperatures and pressures. Eng. Fract. Mech.1985,21, 31–48

[89] Rahimidehgolan, F.; Majzoobi, G.; Alinejad, F.; Fathi Sola, J. Determination of the Constants of GTN Damage Model Using Experiment, Polynomial Regression and Kriging Methods. *Appl. Sci.* **2017**, *7*, 1179.

[90] C. Basaran.; *Introduction to Unified Mechanics Theory with Applications*, Springer-Nature, 2021, ISBN 978-3-030-57772-8

[91] Michael Leukart, Ekkehard Ramm, A comparison of damage models formulated on different material scales, Computational Materials Science, Volume 28, Issues 3–4, 2003, Pages 749-762, ISSN 0927-0256, https://doi.org/10.1016/j.commatsci.2003.08.029.

[92] Mkaddem, A., Hambli, R. & Potiron, A. Comparison between Gurson and Lemaitre damage models in wiping die bending processes. *Int J Adv Manuf Technol* **23,** 451–461 (2004). https://doi.org/10.1007/s00170-003-1701-3

[93] T.-S. Cao, A. Gaillac, P. Montmitonnet, P.-O. Bouchard, Identification methodology and

comparison of phenomenological ductile damage models via hybrid numerical–experimental analysis of fracture experiments conducted on a zirconium alloy, International Journal of Solids and Structures, Volume 50, Issue 24, 2013, Pages 3984-3999, ISSN 0020-7683, https://doi.org/10.1016/j.ijsolstr.2013.08.011.

[94] Mohanraj Murugesan, Seonggi Lee, Dongwook Kim, Youn-Hee Kang, Naksoo Kim,A Comparative Study of Ductile Damage Models Approaches for Joint Strength Prediction in Hot Shear Joining Process, Procedia Engineering, Volume 207, 2017, Pages 1689-1694, ISSN 1877-7058, https://doi.org/10.1016/j.proeng.2017.10.923.

[95] Amaral, R., Teixeira, P., Santos, A.D. *et al.* Assessment of different ductile damage models and experimental validation. *Int J Mater Form* **11,** 435–444 (2018). https://doi.org/10.1007/s12289-017-1381-4

[96] Jun Zhou, Xiaosheng Gao, James C. Sobotka, Bryan A. Webler, Brian V. Cockeram, On the extension of the Gurson-type porous plasticity models for prediction of ductile fracture under shear-dominated conditions, International Journal of Solids and Structures, Volume 51, Issue 18, 2014, Pages 3273-3291, ISSN 0020-7683, https://doi.org/10.1016/j.ijsolstr.2014.05.028.

[97] T. Temfack & C. Basaran (2015) Experimental verification of thermodynamic fatigue life prediction model using entropy as damage metric, Materials Science and Technology, 31:13, 1627-1632, DOI: 10.1179/1743284715Y.0000000074

[98] C. Basaran and R. Chandaroy, "Finite element simulation of the temperature cycling tests," *in* IEEE Transactions on Components, Packaging, and Manufacturing Technology: Part A, vol. 20, no. 4, pp. 530-536, Dec. 1997, doi: 10.1109/95.650944.

[99] Teng, Z. et al. “Thermodynamic entropy as a marker of high-cycle fatigue damage accumulation: Example for normalized SAE 1045 steel.” Fatigue & Fracture of Engineering Materials & Structures (2020): n. pag.

[100] Yun, H.; Modarres, M. Measures of Entropy to Characterize Fatigue Damage in Metallic Materials. *Entropy* **2019**, *21*, 804.

[101] Tvergaard V. and Needleman A. Analysis of the Cup-cone Fracture in a Round Tensile Bar // Acta Metall. - 1984. - 32. - pp. 157-169.

[102] Kachanov, L.M., 1958. On the creep rupture time. Otd. Tehn. Nauki. 8, 26–31 (InRussian; Izv. AN SSSR).

[103] Lemaitre, J., 1996. A Course on Damage Mechanics, 2nd ed. Springer-Verlag, Berlin,Heidelberg, New York.

[104] Chaboche, J.L., 2008. A review of some plasticity and viscoplasticity constitutive theories. Int. J. Plast. 24, 10 1642–1693. https://doi.org/10.1016/j.ijplas.2008.03.009

[105] Basaran C, Chandaroy R., 1998, “Mechanics of Pb40/Sn60 Near-eutectic Solder Alloy Subjected to Vibration”, Applied Math. Modelling, vol.22, pp.601-627.

[106] Peric’, D. On a class of constitutive equations in viscoplasticity: Formulation and computational issues. Int. J. Numer. Methods Eng. **1993**, 36, 1365–1393.

[107] Dongyang Chu, Xiang Li, Zhanli Liu, Junbo Cheng, Tao Wang, Zhijie Li, Zhuo Zhuang, A unified phase field damage model for modeling the brittle-ductile dynamic failure mode transition in metals, Engineering Fracture Mechanics, Volume 212, 2019, Pages 197-209, ISSN 0013-7944, https://doi.org/10.1016/j.engfracmech.2019.03.031.

[108] Schreiber, C., Müller, R. & Kuhn, C. Phase field simulation of fatigue crack propagation under complex load situations. *Arch Appl Mech* (2020). https://doi.org/10.1007/s00419-020-01821-0

[109] Badnava, H.; Etemadi, E.; Msekh, M.A. A Phase Field Model for Rate-Dependent Ductile Fracture. *Metals* **2017**, *7*, 180.

[110] Guo, Qiang & Zaïri, Fahmi & Guo, Xinglin. (2018). An intrinsic dissipation model for high-cycle fatigue life prediction. International Journal of Mechanical Sciences. 140. 10.1016/j.ijmecsci.2018.02.047.

[111] Johnson, J.N., 1981. Dynamic fracture and spallation in ductile solids. Journal of Applied Physics 52 (4), 2812–2825.

[112] Basaran, C., and Chandaroy, R.,"Nonlinear Dynamic Analysis of Surface Mount Interconnects, Part I: Theory", Trans. of ASME, Journal of Electronic Packaging, Vol. 121, Number 1, pp. 8-12, March 1999.

[113] Basaran, C., and Chandaroy, R.,"Nonlinear Dynamic Analysis of Surface Mount Interconnects, Part II: Applications", Trans. of ASME, Journal of Electronic Packaging, Vol. 121, No 1, pp. 12-17, March 1999.

[114] Basaran, C., and Chandaroy, R., "Mechanics of Pb40/Sn60 Near –Eutectic Solder Alloys Subjected to Vibrations," Journal of Applied Mathematical Modeling, Vol. 22, pp. 601-627, 1998,

[115] Basaran, C., and Yan. C.Y."A Thermodynamic Framework for Damage Mechanics of Solder Joints," Trans. of ASME, Journal of Electronic Packaging, Vol. 120, 379-384, 1998.

[116] Chandaroy, R. and Basaran, C.,"Damage Mechanics of Surface Mount Technology Solder Joints Under Concurrent Thermal and Dynamic Loadings," Trans. of ASME, Journal of Electronic Packaging, Vol. 121, pp. 61-68, 1999.

[117] Basaran, C. and Chandaroy, R.,"Thermomechanical Analysis of Solder Joints Under Thermal and Vibrational Loading," Tran. ASME Journal of Electronic Packaging, Vol. 124, No 1, pp. 60-67, March 2002.

[118] Tang, H. and Basaran, C."Influence of Microstructure Coarsening on Thermomechanical Fatigue Behavior of Pb/Sn Eutectic Solder Joints," Int. Journal of Damage Mechanics, Vol. 10, No 3, pp. 235-255, July 2001.

[119] Basaran, C. and Tang, H.,"Implementation of a Thermodynamic Framework for Damage Mechanics of Solder Interconnects in Microelectronic Packaging," International Journal of Damage Mechanics, Vol. 11, No. 1, pp. 87-108, January 2002.

[120] Tang, H. and Basaran, C."A Damage Mechanics Based Fatigue Life Prediction Model," Trans. Of ASME, Journal of Electronic Packaging, Vol. 125, No 1, pp. 120-125, March 2003.

[121] Basaran, C. and Nie, S.”An Irreversible Thermodynamic Theory for Damage Mechanics of Solids,” International Journal of Damage Mechanics, vol. 13, No 3, pp 205-224, July 2004,

[122] Gomez, J. and Basaran, C.”A Thermodynamics Based Damage Mechanics Constitutive Model for Low Cycle Fatigue Analysis of Microelectronics Solder Joints Incorporating Size Effect,” International Journal of Solids and Structures, Vol. 42, issue 13, pp. 3744-3772, (2005)

[123] Basaran, C. and Nie, S.”An Irreversible Thermodynamic Theory for Damage Mechanics of Solids,” International Journal of Damage Mechanics, vol. 13, No 3, pp 205-224, July 2004,

[124] Gomez, J. and Basaran, C.”A Thermodynamics Based Damage Mechanics Constitutive Model for Low Cycle Fatigue Analysis of Microelectronics Solder Joints Incorporating Size Effect,” International Journal of Solids and Structures, Vol. 42, issue 13, pp. 3744-3772, (2005)

[125] Gomez, J. and Basaran, C.”A Thermodynamics Based Damage Mechanics Constitutive Model for Low Cycle Fatigue Analysis of Microelectronics Solder Joints Incorporating Size Effect,” International Journal of Solids and Structures, Vol. 42, issue 13, pp. 3744-3772, (2005

[126] Gomez, J. and Basaran, C.”A Thermodynamics Based Damage Mechanics Constitutive Model for Low Cycle Fatigue Analysis of Microelectronics Solder Joints Incorporating Size Effect,” International Journal of Solids and Structures, Vol. 42, issue 13, pp. 3744-3772, (2005)

[127] Basaran, C., Zhao, Y., Tang, H. and Gomez, J..”A Damage Mechanics Based Unified Constitutive Model for Solder Alloys,” Trans of ASME, Journal of Electronic Packaging, Vol. 127, issue 3, pp. 208-214, September 2005 .

[128] Gomez, J. and Basaran, C. “ Nanoindentation of Pb/Sn Solder Alloys; Experimental and Finite Element Simulation Results”, Int. J. of Solids and Structures, vol. 43, (2006), pp. 1505-1527, 2006,

[129] Gomez, J. and Basaran, C., ”Damage Mechanics Constitutive Model for Pb/Sn Solder Joints Incorporating Nonlinear Kinematic Hardening and Rate Dependent Effects Using a Return Mapping Integration Algorithm,” Mechanics of Materials, 38 (2006), 585-598.

[130] Gomez, J, Lin, M. and Basaran, C. “Damage Mechanics Modeling of Concurrent Thermal And Vibration Loading On Electronics Packaging” Multidiscipline Modeling in Materials and Structures, Vol.2, No.3, pp. 309-326, July 2006.

[131] Therence Temfack, Cemal Basaran, “Experimental Verification of a Thermodynamic Fatigue Life Prediction Model” Materials Science and Technology, Volume 31, Issue 13, 2015,

[132] Bin Jamal, N., Kumar, A., Rao, L., Basaran, C. “Low Cycle Fatigue Life Prediction Using Unified Mechanics Theory in Ti-6Al-4V Alloys”, Entropy 2020, 22(1), 24;

[133] Bin Jamal, N., Rao, L., Basaran, C., “A unified mechanics theory-based model for temperature and strain rate dependent proportionality limit stress of mild steel”, Mechanics of Materials, 155, (2021),103762

[134] Bin Jamal, N., Lee, H.W., Rao, L., Basaran, C.” Dynamic Equilibrium Equations in Unified Mechanics Theory” Applied Mechanics (submitted January 26, 2021)

[135] Lee, H.W., Basaran, C. "Predicting High Cycle Fatigue Life with Unified Mechanics Theory," Int. J. of Fatigue (Submitted January 27, 2021)

[136] Basaran, C., Lin, M. and Ye. H. "A Thermodynamic Model for Electrical Current Induced Damage", Int. Journal of Solids and Structures Vol. 40, No 26 pp. 7315-7327, November 2003

[137] Lin, M., and Basaran, C."Electromigration Induced Stress Analysis Using Fully Coupled Mechanical-Diffusion Equations With Nonlinear Material Properties," Computational Materials Science, Vol. 34/1 pp. 82-98, May 2005,

[138] Basaran, C. and Lin, M.," Damage Mechanics of Electromigration in Microelectronics Copper Interconnects," International Journal of Materials and Structural Integrity, vol. 1, Nos1/2/3, 16-39, 2007,

[139] Basaran, C. and Lin, M.," Damage Mechanics of Electromigration Induced Failure," Mechanics of Materials, 40 (2008) 66-79,

[140] Abdulhamid, M., Li, S., Basaran, C. "Thermomigration in lead-free solder joints, Int. J. of Materials and Structural Integrity, Vol. 2, Nos 1 / 2, pp. 11-34, 2008,

[141] Basaran, C., Li, S., Abdulhamid, M.," Thermomigration Induced Degradation in Solder Alloys,", Journal of Applied Physics, 103, 123520 (2008),

[142] Li, S., Abdulhamid, M. and Basaran, C. "Simulating Damage Mechanics of Electromigration and Thermomigration," Simulation: Transactions of the Society for Modeling and Simulation International Vol. 84, Number 8/9, pp. 391-401, August/September 2008,

[143] Li, S. and Basaran, C. "A Computational Damage Mechanics Model for Thermomigration," Mechanics of Materials, vol. 41, issue 3, pp. 271-278, March 2009,

[144] Li, S., Abdulhamid, M., Basaran, C. and Lai, Y.S. "Damage Mechanics of Low Temperature Electromigration and Thermomigration" IEEE Trans. On Advanced Packaging, Vol. 32, No 2, pp., 478-485, May 2009,

[145] Abdulhamid, M., Basaran, C., and Lai, Y.S., "Thermomigration vs. Electromigration in Microelectronics Solder Joints" IEEE Transactions on Advanced Packaging, Vol. 32, No 3, pp. 627-635, August 2009,

[146] Basaran, C., Abdulhamid, M." Low Temperature Electromigration and Thermomigration in Lead-Free Solder Joints," Mechanics of Materials, 41, (2009) 1223-1241

[147] Yao, W. and Basaran, C., " Electromigration Analysis of Solder Joints under AC Load: a Mean Time to Failure Model" J. of Applied Physics, 19 March 2012, Journal of Applied Physics , Vol.111, Issue 6,

[148] Yao, W. and Basaran, C., "Electromigration Damage Mechanics of Lead-Free Solder Joints Under Pulsed DC Loading: A Computational Model" Computational Material Science, 71, (2013) 76-88

[149] Yao, W. and Basaran, C." Damage Mechanics of Electromigration and Thermomigration in Lead-free Solder Alloys under AC: An Experimental Study, "Int. J. of Damage Mechanics, Vol. 23 Issue 2 March 2014, pp. 203-221

[150] Yao, W. and Basaran, C. "Computational Damage Mechanics of Electromigration and Thermomigration" J. of Applied Physics, 114, 103708, (2013),

[151] Basaran, C. and Nie, S."An Irreversible Thermodynamic Theory for Damage Mechanics of Solids," International Journal of Damage Mechanics, vol. 13, No 3, pp 205-224, July 2004,

[152] Nie, S., and Basaran, C. "A Micromechanical Model for Effective Elastic Properties of Particulate Composites with Imperfect Interfacial Bonds," International Journal of Solids and Structures Vol. 42, pp 4179-4191, 2005,

[153] Basaran, C. and Nie, S."A Thermodynamics Based Damage Mechanics Model for Particulate Composites," International Journal of Solids and Structures, 44, (2007) 1099-1114.

[154] Gunel, E.M. and Basaran, C. "Damage Characterization in Non-Isothermal Stretching of Acrylics: Part I Theory" Mechanics of Materials, Volume 43, Issue 12, December 2011, Pages 979–991

[155] Gunel, E.M. and Basaran, C. "Damage Characterization in Non-Isothermal Stretching of Acrylics: Part II Experimental Validation, Mechanics of Materials , Volume 43, Issue 12, December 2011, Pages 992–101

[156] Gunel, E. and Basaran, C., "Influence of Filler Content and Interphase properties on Large Deformation Micromechanics of Particle Filled Acrylics," 57, (2013) 134-146 , Mechanics of Materials

[157] Sosnovskiy LA, Sherbakov SS. On the Development of Mechanothermodynamics as a New Branch of Physics. *Entropy*. 2019; 21(12):1188. https://doi.org/10.3390/e21121188

[158] Wang J, Yao Y. An Entropy-Based Failure Prediction Model for the Creep and Fatigue of Metallic Materials. *Entropy*. 2019; 21(11):1104. https://doi.org/10.3390/e21111104

[159] Young C, Subbarayan G. Maximum Entropy Models for Fatigue Damage in Metals with Application to Low-Cycle Fatigue of Aluminum 2024-T351. *Entropy*. 2019; 21(10):967. https://doi.org/10.3390/e21100967

[160] Yun H, Modarres M. Measures of Entropy to Characterize Fatigue Damage in Metallic Materials. *Entropy*. 2019; 21(8):804. https://doi.org/10.3390/e21080804

[161] Sun F, Zhang W, Wang N, Zhang W. A Copula Entropy Approach to Dependence Measurement for Multiple Degradation Processes. *Entropy*. 2019; 21(8):724. https://doi.org/10.3390/e21080724

[162] Hossein Bahrami, S.H. Hoseini, George Z. Voyiadjis, Fracture investigation of the shape memory alloy using GTN model, Engineering Fracture Mechanics, Volume 216, 2019, 106519, ISSN 0013-7944, https://doi.org/10.1016/j.engfracmech.2019.106519.

[163] Hossein Bahrami, S.H. Hoseini, George Z. Voyiadjis, Fracture analysis of shape memory alloys in martensite and austenite phase based on the voids behavior, Mechanics of Materials, Volume 137, 2019, 103119, ISSN 0167-6636, https://doi.org/10.1016/j.mechmat.2019.103119.

[164] Navid Mozaffari, George Z. Voyiadjis, Phase field based nonlocal anisotropic damage mechanics model, Physica D: Nonlinear Phenomena, Volume 308, 2015, Pages 11-25, ISSN 0167-2789, https://doi.org/10.1016/j.physd.2015.06.003.

[165] Navid Mozaffari, George Z. Voyiadjis, Coupled gradient damage – Viscoplasticty model for ductile materials: Phase field approach, International Journal of Plasticity, Volume 83, 2016, Pages 55-73, ISSN 0749-6419, https://doi.org/10.1016/j.ijplas.2016.04.003.

[166] Shen, F., Voyiadjis, G. Z., Hu, W., and Meng, Q. (2015) Analysis on the fatigue damage evolution of notched specimens with consideration of cyclic plasticity. *Fatigue Fract Engng Mater Struct*, 38: 1194– 1208. doi: 10.1111/ffe.12299.

[167] Boyd JG, Lagoudas DC. A thermodynamic constitutive model for the shape memory materials. Part I. The monolithic shape memory alloys. Int J Plasticity 1996;12(6):805–42.